SSC-171

The Superconducting Super Collider

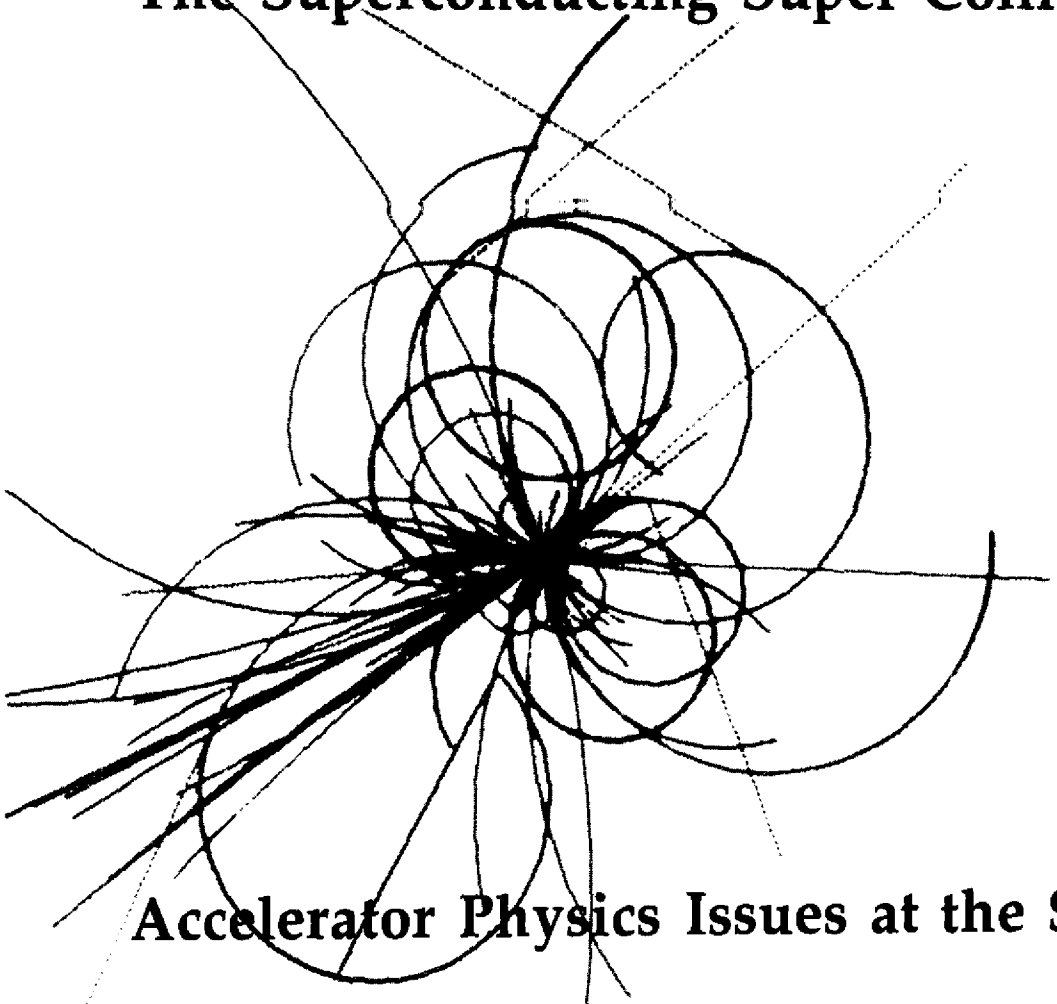

Accelerator Physics Issues at the SSC

D.E. Johnson
SSC Central Design Group

May 1988

SSC-171

ACCELERATOR PHYSICS ISSUES AT THE SSC

D. E. Johnson

SSC Central Design Group*
c/o Lawrence Berkeley Laboratory
Berkeley, CA 94720

May 1988

*Operated by Universities Research Association, Inc. under contract with the U.S. Department of Energy.

ACCELERATOR PHYSICS ISSUES AT THE SSC

D. E. Johnson

SSC Central Design Group
c/o Lawrence Berkeley Laboratory
Berkeley, CA 94720

May 1988

ABSTRACT

The proposed Superconducting Super Collider (SSC) is a high-luminosity proton-proton colliding-beam accelerator, unique in the world, providing access to particle collision energies at least an order of magnitude greater than are available at existing facilities. The design of the SSC has been previously described in the Conceptual Design Report [1]. Although not the final SSC design, this paper updates the previous design to include the changes due to the change in cell phase advance from 60 to 90 degrees, and particularly emphasizes the underlying accelerator physics issues which are involved in the SSC. A brief history of the SSC program is given followed by detailed design considerations.

1. Introduction

The expectation that new phenomena crucial to understanding the fundamental interactions must occur at the 1 TeV energy scale [2] motivates the proposed Superconducting Super Collider, a proton-proton collider with 20 TeV beams and a design luminosity of 10^{33} cm^{-2} s^{-1}.

Several ideas for higher energy accelerators were discussed at the ICFA Workshops on Future Accelerators of 1978 and 1979. The idea of the SSC was born at the Division of Particles and Fields of the American Physical Society Workshop in 1982. There it became clear that to go beyond the Standard Model required hard collisions with sub-energies greater than 1 TeV, and that a multi-TeV hadron collider could be built using the superconducting magnet technology that had been newly won at the Tevatron.

In 1983, workshops at Lawrence Berkeley Laboratory, Cornell University, and the University of Michigan addressed the physics, accelerator, and detector issues associated with such a collider. In the summer of the same year, the High Energy Physics Advisory Panel, which advises the United States Department of Energy (DOE) on particle physics research, unanimously recommended to the DOE that research and development begin immediately, with the goal of realizing multi-TeV hadron collisions at high luminosity as soon as possible. In response, the DOE reprogrammed FY84 funds into SSC magnet research and development.

The following year, a group sponsored by DOE and the directors of the national high-energy physics laboratories prepared a Reference Designs Study, in which three possible designs for the SSC were developed and compared. Based on the conclusions of the Reference Designs Study, the DOE contracted the SSC research and development program with the Universities Research Association, a consortium of 66 leading research universities. The SSC Central Design Group was established, accepted the hospitality of the Lawrence Berkeley Laboratory, and began work on a non-site-specific conceptual design. Experts from many laboratories and universities in the United States and from abroad participated.

The completed Conceptual Design Report, some 700 pages with another 2000 pages of attachments, details the scientific, technical, and cost aspects of the SSC. It was issued in the spring of 1986.

President Reagan endorsed the SSC as a national goal in January, 1987. In April of that year, the Department of Energy began the process of selecting a site for the SSC. From thirty-five proposals that satisfied the basic requirements, a site evaluation committee assembled by the National Academies of Sciences and Engineering made an unranked list of eight "best-qualified" sites. The Department of Energy accepted that list without modification; one site was later withdrawn by the proposer.

The international aspect of the SSC, as contemplated by the Administration, was announced by the DOE on 10 February 1987:

> The Department of Energy will seek cost sharing for the Superconducting Super Collider with all interested countries. Such cost sharing could take the form of in-kind contributions such as magnets or detectors. International interest in the possibility of contributing to the super collider has been expressed specifically in the on-going discussions with the seven other Nations of the Economic Summit. It also has historical precedents....

A statement from the Summary conclusions of the Economic Summit Working Group meeting in 1983 concerning the super collider is significant:

> "Participation of other countries in the construction of [this] accelerator could be envisaged. As is the usual practice in high energy physics, it is anticipated that scientific research will be open to qualified scientists from all countries, with the different countries contributing to the cost of the experimental detectors."

1.1 Brief Description

After being produced by a series of booster accelerators, oppositely directed bunches of protons, each with an energy of 20 TeV, are caused to collide in the SSC, making available a total of 40 TeV of energy in each proton-proton collision. As the protons collide, their constituents can interact. This center-of-mass energy will allow a probing of the 1–2 TeV scale—a frontier energy region believed to be replete with new physics [2]. Since the probability of interaction is comparatively low, the beams can be recirculated to collide repetitively for many hours without significant attenuation. Thus the SSC is constructed as a pair of storage rings capable of holding tightly confined proton beams on closed paths for a day or more without replenishment. The rings are made to cross at six locations where the collisional reactions take place and where detectors that count and measure the reaction products for physics study are located. This

arrangement is shown schematically in Fig. 1. The major design objectives for the SSC are given in Table 1.

Table 1

Primary SSC Design Objectives

Proton beam energy	20 TeV
Luminosity	10^{33} cm^{-2} s^{-1}
Event rate per crossing	1–2
Number of interaction regions	6

The rings confining the proton beams are housed one above another in an underground tunnel that includes the interaction regions. The beams are guided around the desired orbit through an evacuated tube by a system of electromagnets. This magnetic confinement system consists of a periodic array of bending and focusing magnets. The circumference of the rings is 84 km, a size governed by the maximum desired magnetic field of 6.6 tesla and the energy of 20 TeV. The operating cycle of the SSC begins with the collider magnets maintained at a low current for about forty minutes while the proton beams are loaded into both rings. With injection complete, the accelerating system is activated. This final synchronous acceleration is complete in about fifteen minutes when the beams reach their final collision energy of 20 TeV, twenty times the injection energy. The accelerating system is then turned down, the beams are very tightly focused at the interaction points, and the beams are steered into collision. The resulting reactions can be studied for a day or more before the beams are depleted sufficiently so that the cycle must be repeated. The design luminosity is 10^{33} cm^{-2} s^{-1}.

The injector systems consist of a source and linear accelerator chain, followed by three booster synchrotrons in cascade, similar to previous large accelerator complexes. The final booster is a synchrotron with superconducting magnets; the others have conventional copper and iron magnets to permit rapid cycling. In addition to providing protons for the two main rings, the final booster produces external beams for testing the response of detector components before their installation in the interaction regions of the SSC.

2. Primary Parameters

The performance of the SSC can be specified by a relatively small number of primary parameters. To optimize the SSC performance it is necessary first to optimize among these parameters. The design goal is a 20 TeV pp collider storage ring that can achieve a peak luminosity of 10^{33} cm^{-2} s^{-1} with a small number of interactions per bunch-bunch collision.

2.1 Luminosity

The counter-rotating beams in the two collider rings consist of trains of proton bunches, spaced S_B apart, with N_B protons per bunch. The beams are bunched in order to attain the desired luminosity with minimum total beam current and to provide the gaps necessary for aborting the beams. Low current is desirable to minimize beam-gas scattering background, beam stored energy, activation in the dumps and scrapers, irradiation of the electronics, refrigeration power, and stability control requirements.

The luminosity at an interaction region is given for head-on collisions by,

$$\mathcal{L} = N_B^2 c / 4\pi\sigma^2 S_B \tag{2-1}$$

where c is the speed of the beam, taken to be the speed of light, and σ is the rms transverse beam spread (assumed equal in both dimensions) at the interaction point. Note that, with the beam current $I = ec\, N_B/S_B$, the luminosity is proportional to $I^2 S_B$, other parameters held fixed. For a given $\mathcal{L}$, the beam current can be reduced by increasing the bunch spacing. Unfortunately, N_B increases as $\sqrt{S_B}$, causing an increase in the number of interactions per bunch crossing.

The average number of interactions per bunch crossing is

$$\langle n \rangle = \mathcal{L}\ S_B\ \Sigma_{\text{inel}}/c \tag{2-2}$$

where Σ_{inel} is the inelastic proton-proton cross section. The probability that exactly k interactions occur per bunch crossing is given by a Poisson distribution. The corresponding effective luminosity is

$$\mathcal{L}_k = \mathcal{L}\ \frac{\langle n \rangle^k}{k!} \exp(-\langle n \rangle) \tag{2-3}$$

Some experiments may prefer to have one and only one interaction per bunch crossing. The effective luminosity for those experiments is

$$\mathcal{L}_1 = \mathcal{L}\ \langle n \rangle \exp(-\langle n \rangle) \tag{2-4}$$

With $\mathcal{L} = 10^{33}\ \text{cm}^{-2}\ \text{s}^{-1}$ and $\Sigma_{\text{inel}} = 90$ mb given, $\langle n \rangle$ and $\mathcal{L}_1$ are directly related to S_B, as shown in Fig. 2. For a given $\mathcal{L}$, maximum $\mathcal{L}_1$ occurs when $\langle n \rangle = 1$, which corresponds to $S_B = 3.3$ m. The conceptual design has a bunch spacing of 5.1 m, corresponding to $\langle n \rangle \approx 1.7$ and $\mathcal{L}_1 = 0.31 \times 10^{33}\ \text{cm}^{-2}\ \text{s}^{-1}$. The loss in $\mathcal{L}_1$ from choosing $\langle n \rangle = 1.7$ rather than $\langle n \rangle = 1$ is about 14%.

2.2 Other Primary Parameters

The bunch spacing S_B, the number of protons per bunch N_B, and the rms transverse radius of the beam at the interaction point σ have already been discussed. Together they define the luminosity $\mathcal{L}$, Eq. (2-1). Other primary parameters are the betatron amplitude function at the interaction point β^*, the normalized beam emittance ε_N, the total number of protons in each ring N_T, the synchrotron radiation power P, the beam-beam tune shift (head-on $\Delta\nu_{HO}$, and long-range $\Delta\nu_{LR}$), and the partial beam lifetime from proton-proton collisions τ_{pp}. For a given choice of maximum proton energy, luminosity, ring circumference, and bending radius, all the parameters can be expressed in terms of a few,

chosen here to be ε_N, β^*, and S_B. These parameters are then set through an optimization constrained by accelerator physics and detector and accelerator technology. The bending radius (10.1 km) and the circumference (84 km) are set by technological and economic considerations.

2.2.1 Betatron Amplitude Function

The transverse particle motion through the bending and focusing magnets of the confinement system, is conveniently described in terms of the betatron amplitude function or beta function $\beta(s)$, where s is the longitudinal distance around the ring. The envelope of transverse oscillations of the protons about the equilibrium closed orbit is proportional to $\sqrt{\beta(s)}$. To maximize the specific luminosity the beams must be focused to a small transverse size at the interaction points. Thus the confinement system must make $\beta(s)$ small there. The special value of $\beta(s)$ at an interaction point is denoted by β^*.

2.2.2 Normalized Beam Emittance

The normalized transverse emittance ε_N is a measure of the phase space area of the beam in either of the two transverse degrees of freedom. A particle undergoing betatron oscillations with amplitude a has a canonically conjugate momentum amplitude $a\gamma mc/\beta(s)$ where m is the particle's rest mass and $\gamma = E/mc^2$. Assuming independent motion in the two transverse dimensions, the particle will be confined to an area $\pi a^2\gamma mc/\beta(s)$ in phase space in one transverse dimension. A real beam contains particles with many different amplitudes and phases. At a given position around the ring, the particles in the beam have a transverse spread with an rms value σ in one dimension. The normalized emittance ε_N is defined to be the phase space area for $a = \sigma$, divided by πmc. Thus,

$$\varepsilon_N = \gamma\sigma^2/\beta^* \tag{2-5}$$

where σ and β^* are chosen for convenience to be the values at an interaction point. The dimensions of ε_N are length; the common unit is μm or mm-mrad. By virtue of Liouville's theorem and the adiabatic invariance of phase space, ε_N is an invariant quantity for one-dimensional motion unless there are spatially non-uniform fields or sudden changes in the environment of the beam as it moves through the sequence of accelerators of the SSC. Since the beta function is a property of the lattice, it follows that specification of the luminosity, and hence σ, determines the requirement for the normalized beam emittance. This in turn sets requirements on the injector system.

Experience shows that the beam particles are distributed in an approximately Gaussian fashion. The transverse phase space area $\pi\varepsilon_N$, with ε_N given by (2-5), then corresponds to a radius $R = \sigma$ in coordinate space that contains approximately 39% of the beam inside it.

2.2.3 Total Number of Particles

The bunched beam has N_B protons per bunch with spacing S_B. If the circumference of the ring is C and there are no gaps in the bunch train, there are C/S_B bunches present and the total number of protons is

$$N_T = CN_B/S_B \tag{2-6}$$

The total number of protons and the circumference determine the time-averaged beam current, $I = ec\ N_T/C$, where e is the proton's electric charge. N_T also enters linearly in the amount of synchrotron power that must be removed by the refrigeration system. The SSC design has C = 83.631 km and S_B = 5.1 m, corresponding to 16,470 bunches per ring, ignoring the injection and abort gaps.

2.2.4 Synchrotron Radiation Power

A single relativistic particle moving along a path with instantaneous radius of curvature ρ gives off synchrotron radiation at a rate, in SI units,

$$P = \frac{Z_0}{6\pi}\frac{e^2c^2\gamma^4}{\rho^2} \tag{2-7a}$$

where $Z_0 = \sqrt{\mu_o/\varepsilon_o}$ = 377 ohms is the impedance of free space. In the SSC, the bending is not continuous, but is interrupted by gaps between magnets, drift spaces, etc. The average power per particle is therefore diminished by a factor $(2\pi\rho/C)$. The assumption of incoherent emission by all the protons leads to an expression for the total synchrotron radiation power per ring

$$P = \frac{Z_0}{3}\frac{e^2c^2\gamma^4}{C\rho}N_T \tag{2-7b}$$

At 20 TeV, the bending radius corresponding to 6.6 T is 10.1 km. Numerically, the power is P (kW) $\approx 7 \times 10^{-14} N_T$.

2.2.5 Beam-Beam Tune Shift

As the two beams collide head-on the particles in one beam are defocused by the collective electromagnetic field of the other. This highly nonlinear focusing is characterized by a tune shift [3] given explicitly by

$$\Delta\nu_{HO} = N_B r_p/4\pi\varepsilon_N \tag{2-8}$$

where r_p is the classical proton radius. Too large a value of $\Delta\nu_{HO}$ causes the motion of individual beam particles to become unstable. A $\Delta\nu_{HO}$ per crossing point of about 0.004 (cumulative total tune spread of 0.024 for six crossing points) is the experimentally determined limit in the Sp$\bar{p}$S operating in the colliding mode [4]. Similar figures should be achievable in the SSC, if need be. The current design, however, results in a tune spread of less than 0.001 per crossing point.

In addition, because the bunch spacing is short compared with the field-free space on either side of the crossing point, bunches in one beam are subjected to several close encounters with bunches in the counter-streaming beam while traversing the field free

region. This interaction, which is inversely proportional to the center-to-center distance of the bunches as they pass, results in an equilibrium orbit distortion and a shift in single particle tune called the long range beam-beam tune shift. The value of this tune shift for particles executing small-amplitude betatron oscillations is [5]

$$\Delta\nu_{LR} = \Delta\nu_{HO}\ 2n\,(\sigma/\beta^*\,\alpha)^2 = N_B\, r_p\, n\,/2\pi\gamma\beta^*\,\alpha^2 \tag{2-9}$$

where n is the number of long-range encounters in the interaction region and α is the crossing angle between the two beam trajectories. The nominal values for the SSC are α = 75 μrad, with S_B = 5.1 meters and n = 63 and 131 for the high-luminosity and medium-luminosity regions, respectively. For high luminosity operations in the SSC, the linear tune shift from the long-range beam-beam interactions is about twice that caused by the head-on interactions. The tune spread and its associated nonlinear effects are, however, not as strong as their head-on counterparts.

2.2.6 Partial Beam Lifetime from Proton-Proton Collisions

As the beams collide to produce physically interesting interactions, particles are lost from the bunches. The corresponding beam lifetime, referred to as the partial beam lifetime from proton-proton collisions, is

$$\tau_{pp} = N_T / n_{\mathcal{L}}\ \mathcal{L}\ \ \Sigma_{\text{inel}} \tag{2-10}$$

where $n_{\mathcal{L}}$ is the effective number of interaction regions that utilize the full luminosity of $\mathcal{L}$. Here $n_{\mathcal{L}}$ = 2.1 and Σ_{inel} = 90 mb are representative values.

2.3 Effects of Variation of Parameters

The design requirements of the SSC set limits on the various accelerator physics parameters of the machine or, conversely, the choice of a few basic parameters largely determines the overall characteristics of the accelerator. The inter-relationships among the primary parameters, assuming that E = 20 TeV, $\mathcal{L}$ = 10^{33} cm^{-2} s^{-1} at 20 TeV per beam, circumference C = 84 km, that there are no gaps in the beams, and that ρ = 10.1 km are explored below.

2.3.1 Basic Equations

The parameters σ, N_B, N_T, P, τ_{pp}, $\Delta\nu_{HO}$ and $\Delta\nu_{LR}$, are expressed as functions of β^*, ε_N and S_B using the above relations. The numerical expressions, at 20 TeV, are

$$\sigma[\mu\text{m}] = 6.85\ (\varepsilon_N\,\beta^*)^{1/2}$$

$$N_B\ [10^{10}] = 0.44\ (\varepsilon_N\,\beta^*)^{1/2}\, S_B^{1/2}$$

$$N_T\ [10^{14}] = 3.71\ (\varepsilon_N\,\beta^*)^{1/2}\, S_B^{-1/2}$$

$$I\ (\text{mA}) = 213\ (\varepsilon_N\,\beta^*)^{1/2}\, S_B^{-1/2}$$

$$P\ [\text{kW}] = 26\ (\varepsilon_N\,\beta^*)^{1/2}\, S_B^{-1/2} \tag{2-11}$$

$$\tau_{pp}\ [\mathrm{h}] = 545\ (\varepsilon_N \beta^*)^{1/2}\, S_B^{-1/2}$$

$$\Delta\nu_{HO}\ [10^{-3}] = 0.54\ (\beta^*/\varepsilon_N)^{1/2}\, S_B^{1/2}$$

where ε_N is in units of μm-rad, β^* and S_B are in meters. The units of the dependent quantities are indicated in the square brackets on the left. Strictly speaking, the expressions are valid only for head-on collisions, but the changes for finite crossing angle are known and small (see below Eq. (2-13)).

The long-range beam-beam tune shift depends on additional quantities, i.e., the crossing angle α and the number of long range encounters per interaction region, n. The values of $\alpha = 75$ μrad and $n = 63 \times (5.1\ \mathrm{m}/S_B)$ for the high-luminosity interaction region yield

$$\Delta\nu_{LR}\ [10^{-3}] = 2.9\ (\beta^*/\varepsilon_N)^{-1/2}\, S_B^{-1/2} \tag{2-12}$$

The first six quantities in Eq. (2-11) are functions of the product $\varepsilon_N \beta^*$ through the beam size at the interaction point. The two beam-beam tune shifts $\Delta\nu_{HO}$ and $\Delta\nu_{LR}$ are functions of β^*/ε_N.

2.3.2 Variation of β^* and ε_N

Reducing the product $\varepsilon_N \beta^*$ reduces the needed beam current for a given luminosity. Although reduced $\varepsilon_N \beta^*$ results in a smaller τ_{pp} and a smaller beam size and thus tighter position tolerances, most of the effects of reduced beam current are advantageous. Thus the smallest values of ε_N and β^* commensurate with the conservative application of current technology are chosen: $\varepsilon_N = 1$ μm–rad and $\beta^* = 0.5$ m. The minimum possible value of ε_N is set by achievable ion source brightness. Sources capable of current adequate for SSC purposes have $\varepsilon_N = 0.1$ μm–rad, sufficiently bright to permit the design emittance in the collider. The minimum practical value of β^* is set in this instance by the maximum obtainable quadrupole gradient and aperture considerations. Use of special materials or lower temperatures in the final-focus quadrupoles or shortening the experimental free space may make lower values of β^* possible. The choices of ε_N and β^* also affect the beam-beam tune shifts. In the present case, however, the tune shifts are well below the projected limits and changes of a factor of two in ε_N or β^* result in only a 5% change in total tune shift.

2.3.3 Variation of S_B

Having fixed the design values of $\beta^* = 0.5$ m and $\varepsilon_N = 1$ μm-rad, we must select S_B through optimization among conflicting essentials. The important considerations are shown graphically in Figs. 2 and 3(a) and (b). The rf frequency and relative lengths of the arcs and straight sections have been chosen so that many different bunch spacings are possible. The design chosen is consistent with operation close to the peak of $\mathcal{L}_1$, the effective luminosity for one event per crossing. By moving slightly off the peak at S_B = 3. m to 5.1 m a gain about 50% in the repetition time for the detectors (from 11 to 17 ns) can be realized and a significant saving in synchrotron radiation power and in bandwidth

required for the bunch-by-bunch feedback system can be obtained, while losing only 14% in $\mathcal{L}_1$. At $S_B = 5.1$ meters and an rf frequency of 354 MHz, every sixth bucket is filled.

2.3.4 Energy Dependences

Luminosity at energies other than 20 TeV depends on whether it is limited by the beam-beam tune shift or by the average number of interactions per bunch crossing. Since the head-on beam-beam tune shift at 20 TeV is 0.86×10^{-3}, smaller than the value 4×10^{-3} estimated to be the beam-beam stability limit, the operation at high energies is not beam-beam instability-limited. At 20 TeV, the beam intensity is also limited by the cryogenic system capacity to absorb synchrotron radiation. As the beam energy is lowered from 20 TeV with constant synchrotron radiation power, the beam intensity can increase as $N_B \propto E^{-4}$, leading to a luminosity increase which is $\mathcal{L} \propto E^{-7}$, and $\langle n \rangle \propto E^{-7}$. However, growth of N_B is limited by the capabilities of the injector system and the sharp increase in $\langle n \rangle$ is presumably not acceptable for the detectors. A more realistic scenario is to keep $\mathcal{L}$ and $\langle n \rangle$ constant as E is lowered from 20 TeV. Then, $N_B \propto E^{-1/2}$, $\Delta\nu_{HO} \propto E^{-1/2}$, and $\Delta\nu_{LR} \propto E^{-3/2}$. Figure 4 shows the energy dependence of these parameters in this scenario of operation.

As the beam energy is reduced the head-on beam-beam tune shift does not reach 4×10^{-3} until the beam energy is lowered to 1 TeV. The long-range beam-beam tune shift, however, increases rapidly as the energy is lowered. In the scenario shown in Fig. 4 the beam-beam limit is reached when the *total* tune shift per crossing $\Delta\nu_t$ is 5×10^{-3}. This occurs at 11.2 TeV. As the beam energy is further reduced, it is possible to keep the long-range beam-beam tune shift constant by increasing the crossing angle with the scaling $\alpha \propto E^{-1/2}$. Below 11.2 TeV, $\Delta\nu_t$ = constant, N_B = constant, $\mathcal{L} \propto E$ and $\langle n \rangle \propto E$. These behaviors are also shown in Fig. 4. At the lowest energies (below about 2 TeV), there might be practical restrictions on the crossing angle. If so, the luminosity will be somewhat reduced from that shown in Fig. 4.

2.3.5 Crossing Angle

To enjoy the benefits of relatively small S_B, the beams must cross at an angle to avoid having more than one collision in each experimental straight section. A small reduction in luminosity results [6]

$$R \equiv \frac{\mathcal{L}}{\mathcal{L}_o} = \frac{1}{\sqrt{1 + (\alpha\sigma_z/2\sigma)^2}} \tag{2-13}$$

where σ_z is the longitudinal rms bunch dimension. The effect is small even in the high luminosity interaction regions where it is most pronounced. To maintain a given $\mathcal{L}$, the quantity N_B (and consequently N_T, I, P, τ_{pp}, and $\Delta\nu_{LR}$) must be increased by a factor $R^{-1/2}$. With α = 75 μrad, σ_z = 7 cm, and σ = 4.8 μm, the increase in N_B is 7%. The needed increase for the intermediate luminosity case is hardly noticeable.

A finite crossing angle also slightly affects the head-on beam-beam tune shift. The tune shift in the crossing plane is [6]

$$(\Delta\nu_{HO})_{\text{crossing plane}} = \frac{N_B r_p}{4\pi\varepsilon_N}\left[\frac{2R^2}{1+R}\right] , \tag{2-14a}$$

while in the non-crossing plane, it is

$$(\Delta\nu_{HO})_{\text{noncrossing plane}} = \frac{N_B r_p}{4\pi\varepsilon_N}\left[\frac{2R}{1+R}\right] . \tag{2-14b}$$

Finally, the bunch filling factor must be included in the above calculations. This is the ratio of the number of bunches actually in the machine to the maximum possible number of bunches. The filling factor is less than unity due to the need to have gaps in the beam for kicker rise and fall times, etc. In the SSC this factor is FF = 0.938.

The values of quantities listed in Eq. (2-11) are given below, taking into account the crossing angle effects ($\beta^* = 0.5$ m, $\varepsilon_N = 1$ μm-rad, $\alpha = 75$ μrad and $\sigma_z = 7$ cm) and the filling factor [7]

$$\begin{aligned}
&R = 0.88\\
&\sigma = 4.8\ \mu\text{m}\\
&N_B = 8.01 \times 10^9\\
&N_T = 1.24 \times 10^{14}\\
&I = 71\ \text{mA}\\
&P = 8.9\ \text{kW}\\
&\tau_{pp} = 181\ \text{h}\\
&(\Delta\nu_{HO})_{\text{crossing plane}} = 0.81 \times 10^{-3}\\
&(\Delta\nu_{HO})_{\text{noncrossing plane}} = 0.92 \times 10^{-3}\\
&\Delta\nu_{LR} = 2.0 \times 10^{-3}
\end{aligned} \tag{2-15}$$

The synchrotron radiation power listed includes the additional 0.09 kW contribution from the beam separation dipoles on each side of the interaction points.

It should be stressed that the values of Eq. (2-15) are nominal. There is considerable flexibility in crossing angle, bunch spacing, and other parameters to provide optimal conditions in actual operation.

3. Lattice

The lattice design of the SSC is critical because of the variety of experimental and operational needs it must accommodate while minimizing intrinsic nonlinearities in the designed ideal structure, sensitivity of particle motion to various errors, and cost.

The lattice of the SSC has a racetrack shape with eight straight sections placed in two clusters of four each. The straight sections are made of two general types of modules: interaction regions (IRs) and utility modules. Designating these modules by X and U, respectively, the SSC lattice consists of the following sequence: *F, F, X, X, Arc, U, U, X, X, Arc*, where F indicates a future interaction region that at present has the lattice structure of a utility section. See Fig. 1. The IR and the utility modules are interchangeable from the lattice design point of view. They both have lengths of 2285 m and both match to the optical functions of the basic arc cells at their ends.

The IRs are arranged in two clusters, 2 IRs and 2 utilities in one cluster, called the Near Cluster, and 4 IRs in the other (Far) Cluster. The clustered IRs are adopted for the SSC to permit extensive sharing of support facilities. The Near and Far Clusters are connected by regular bending arcs, each of which contains 143 identical FODO cells.

There are two different types of interaction regions where the beams cross vertically and the beams are strongly focused by quadrupole triplets on either side of the interaction point (IP). The IRs in the Near Cluster are designed for high luminosity operation and the interaction point has $\beta^*_x = \beta^*_y = 0.5$ m, a luminosity of 10^{33} cm^{-2} s^{-1}, and a distance between the IP and the face of the first IR quadrupole of $L^* = 20$ m. The last 3 m of this 20 m space contains parts of cryogenic systems and scrapers to protect the triplet quadrupoles from the secondary beam radiation. The maximum beta function in the triplet is about 8000 m. The IRs in the Far Cluster are designed to provide intermediate luminosities. Here the interaction point has $\beta^* = 10$ m and the free space around the interaction point is ±120 m; the luminosity is 0.56×10^{32} cm^{-2} s^{-1}. The flexibility of the lattice design permits continuous evolution of the interaction region layout to optimize experimental usage over the life of the facility. During colliding beam operations, the luminosity of an individual low-beta IR can be controlled by adjusting β^* between 0.5 m and 8 m, while the medium-beta IRs can be tuned over the range of β^* between 10 m and 60 m, the latter values being those used for injection.

The choice of $\beta^* = 0.5$ m for high-luminosity operations depends on the value of $L^* = 20$ m. The possibility of shortening L^* to allow a lower value of β^*, and thus higher luminosity without increasing the beam intensity, has been studied [8]. Reducing L^* to 15 m would allow β^* to be lowered to about 0.4 m with an increase of the maximum beta function or an increase in the maximum strength in the triplet quadrupoles. With $\alpha = 75$ μrad and $\sigma_z = 7$ cm, this allows the luminosity to increase by 25%. Increasing L^* to 25 m, on the other hand, would cause β^* to increase to 0.65 m, thus reducing the luminosity by about 20%.

The beams cross each other with a small angle at the interaction points. The angle is typically 75 μrad but is variable from 0 to 150 μrad or higher. The final focusing triplets are shared by both beams. After the triplet the beams are separated vertically in two stages to a separation of 70 cm. The section that provides the beam separation also

matches and removes vertical dispersion. The horizontal dispersion is then matched to the regular arc cell values by another section that also matches the betatron functions.

The remaining modules are the utility modules. The two in the Near Cluster have free space available for the beam injection and abort systems. The rf cavities, occupying a total space of 25 meters per ring, are also located in the utility sections, along with several sets of beam scrapers and collimators.

Each module structure is antisymmetric about the center of the straight section: it is mirror symmetric about that point, but the signs of the corresponding quadrupole gradients are opposite.

The modules are identical in length and horizontal bending angle, and have betatron phase advances equal to odd multiples of $\pi/2$ (which do not change between injection and collision optics). These phases are chosen to produce partial cancellation of chromatic perturbations between pairs of identical modules.

3.1 Lattice Considerations

For high luminosity operation and assumed equal horizontal and vertical emittances, the beam at the interaction point (IP) is round, with $\beta^*_x = \beta^*_y = 0.5$ m. On each side of an IP, a triplet of quadrupoles is used to provide the strong focusing needed at the IP [9,10]. This allows the maximum beta function in the interaction region (IR) quadrupoles to be minimized. The magnet polarities are antisymmetric about the IPs. This simplifies the IR design since a symmetric design necessarily requires two types of IRs.

The distance between the IP and the face of the first IR quadrupole is $L^* = 20$ m. This gives maximum beta function values in the triplet of about 8 km in the colliding mode with $\beta^* = 0.5$ m. The nonlinear chromatic effects introduced by this IR insertion are relatively small compared with those introduced by the arc dipole magnets (with their field errors), and the beam energy spread is small ($\sigma_\delta = 0.5 \times 10^{-4}$). Thus the major consequences of the relatively large maximum beta are tightened alignment and magnet field error tolerances. A beam-steering feedback system based on a scanned luminosity measurement as its input signal will secure the needed alignment. Special multipole correction circuits in the triplet quadrupoles are used to compensate for the magnet field error effect.

The beams are separated vertically by 70 cm in the arcs. The magnets in the arcs are arranged in an over-under configuration. The 70 cm separation allows the magnets of the two rings to be decoupled cryogenically as well as magnetically. The over-under arrangement allows the tunnel space to be utilized effectively and allows the path lengths between collision points in the two rings to be easily equalized. The decoupled magnets allow separate operation of the two rings. Among other things, this makes it possible to perform accelerator physics studies on one ring when the other ring is not available [11].

The suppression of the vertical dispersion introduced by the separation section is accomplished by dividing the 70 cm separation into two steps and then introducing a bend-free section which has 180 degree phase advance between the two steps. The vertical dispersion contributions from the two steps cancel outside the separation region.

Tune variations are obtained by varying the two families of trim quadrupole coils in the corrector spool packages. The range of the tune variation is ±2 units in each plane. The phase advance per cell then deviates slightly from 90 degrees, but this deviation does not cause reduction in beam aperture. This tune variation does not effect the phase advance between IRs. Further, it is possible to keep the optimal advance between adjacent IPs in a cluster fixed when β^* is varied from injection to collision values.

3.2 Clustered Interaction Regions

The beam optics, beam-beam effects, and background radiation are some of the accelerator physics issues to be considered when discussing clustered interaction regions. The results of a study of these questions [12] are summarized in the present section. The main conclusion of the study is that both distributed and clustered IRs are acceptable for the SSC design from the accelerator physics point of view. However, the clustered scheme is more cost effective because of considerations concerning the conventional facilities.

Generally speaking, evenly distributed IRs permit a higher superperiodicity and thus fewer systematic resonances in the tune space. For the case of SSC, this means a superperiodicity of 6, if the utility sections and crossings are ignored. Realization of the consequences of high superperiodicity requires correlation of particle motion in magnets that are separated by 1/6 of the ring circumference, nearly 14 km. Because of various magnet field and alignment errors, correlation over this long distance is not likely to be maintained. The superperiodicity is thus broken in reality and all low-order resonances, systematic and accidental, need to be avoided.

Particle tracking programs have been used to demonstrate that high superperiodicity is not very important for the SSC. The maximum amplitude of stable motion (referred to as the dynamic aperture) has been studied as a function of momentum deviation $\delta = \Delta E/E$. Random magnet multipole errors are included in these simulations. For each case, the same tunes are used, away from systematic resonances. The dependence of dynamic aperture on the IR layout, and thus the superperiodicity, is not significant.

The betatron phase advance per cell in general depends on the momentum deviation δ. This dependence of the phase advance is specified by the chromaticity, i.e., the derivative of the phase advance with respect to δ, divided by 2π. In a storage ring with IRs, chromaticity accumulates over an interaction region, but is reset to zero by properly setting the two families of chromaticity sextupoles in the adjacent arcs. This is done for all IR layouts. However, for the clustered layout, the chromaticity accumulates over a few IRs before it is corrected in the arcs. A possible undesirable effect of this is a betatron phase modulation of the beam-beam kicks because of synchrotron oscillation. The amplitude of the phase modulation, however, is only about 0.6 degrees for a particle executing a synchrotron oscillation with amplitude of $\delta = 10^{-4}$. Such a phase modulation is negligible compared with that due to the beam-beam effects. The possibility of having multiple sextupole families rather than two to control the chromaticities locally has been studied for various clustering arrangements [13]. The chromatic behavior in general was found to deteriorate as compared with the two family scheme.

There is an optical advantage of IR clustering. Compared with distributed IRs, clustered IR lattices have one more variable to control the optical quality, namely, the

betatron phase advance μ between adjacent IPs in a cluster. The optimum value of μ is found to be an odd multiple of $\pi/2$ [12, 14, 15]. By pairing IRs in a cluster and setting μ to the optimum value, the chromatic aberrations of particle motion can be minimized. This optimum phase also helps to reduce the orbit effect from long-range beam-beam interactions and to suppress some of the incoherent beam-beam resonances.

The tune dependence on momentum is described to first order by the chromaticity. As mentioned, the chromaticity is set to zero by properly setting the two families of chromaticity sextupoles in the arcs. The second order dependence of the tune on momentum could be removed by introducing multiple sextupole families, but it is also substantially reduced if adjacent IRs are paired with $\mu = (2n+1)\pi/2$. The condition of $\mu = (2n+1)\pi/2$ also minimizes the energy dependence of β^* and the beta function in the triplets, which in turn minimizes the spurious dispersion at the interaction point from misalignment of the IR quadrupoles [12].

3.3 Arcs

The arc cells are regular FODO cells with a length of 228.5 m, each consisting of 12 bending magnets and two quadrupole magnets, as shown in Fig. 5. The cell has a nominal focusing phase advance of 90 degrees. The bending magnet field at 20 TeV is 6.6 T. The quadrupole gradient is 230 T/m.

The cell length of 228.5 m is a result of cost minimization, given the aperture needed for stability of particle motion. The betatron phase advance per cell in the CDR was taken to be 60 degrees. An extensive study was undertaken to determine the optimal phase advance per cell in the presence of magnet field errors [16]. It was found that a 90 degree phase advance was better optically for a given cell length. A comparison was made between the CDR case of 60 degree phase advance with 100 m cells and a 90 degree, 120 m cell case. It was found that the two alternatives are quite comparable in performance. The 60 degree phase advance gives better on-momentum behavior, but worse off-momentum behavior, than does the 90 degree case. Both choices provide acceptable aperture for stable particle motion, although the better off-momentum behavior of the 90 degree choice is slightly preferred.

In each cell, two spaces are reserved for so-called spool pieces where various correction coil packages, as well as cryogenic connections, are located. Orbit distortions, for example, are corrected by dipole correctors, while the phase advance per cell can be varied by trim quadrupoles in the spool pieces. The range of variation of phase corresponds to a tune variation of ± 2 units. Two families of chromaticity sextupoles are also included in the spool pieces. In addition, several multipole correctors are available in the spool pieces to stabilize particle motion in the presence of the nonlinear magnet field errors.

There are two arc modules in the SSC, each consisting of 143 cells. With a 90 degree phase advance and 228.5 m length per cell, an arc module has a tune contribution of 35 3/4 and a length of 32675.5 m. Six bending magnets, each with magnetic length of 16.54 m, are placed between adjacent quadrupoles. The corresponding magnets of the two rings are placed exactly above and below each other, separated by 70 cm. The two quadrupoles at a given longitudinal position have the same gradient but opposite focusing effect on the two beams.

In order to make room for the correction spool pieces, the group of six bending magnets is shifted (in the same direction in all cells) by 2.89 m away from the center of the drift space. This shift does not affect the beta functions but slightly alters the dispersion function, giving rise to a finite slope at the centers of the focusing and defocusing quadrupoles. To the extent that this perturbed dispersion needs to be corrected, it can be matched into the utility and IR modules by their dispersion suppressor quadrupoles.

3.4 Interaction Region Modules

It is envisioned that the SSC will eventually have six IRs. Initially, however, only four will be used. An attractive possibility, adopted for the conceptual design, is to have two IRs with high luminosities (10^{33} cm^{-2}s^{-1}) and two with intermediate luminosities (0.56×10^{32} cm^{-2}s^{-1}). The high-luminosity module has $\beta^* = 0.5$ m and a free space $L^* = \pm 20$ m about the IP, while the intermediate-luminosity module has $\beta^* = 10$ m and a much longer free space $L^* = \pm 120$ m. The value of $\beta^* = 0.5$ m for the high-luminosity module is believed to be close to the tightest focusing allowed by the presently obtainable quadrupole gradients. On the other hand, $\beta^* = 10$ m for the intermediate-luminosity module is somewhat flexible. The two initially unused IRs are simply represented by utility sections in this design.

Except for an added half cell at one end, an IR module is centered about the interaction point (IP) and is optically matched to link to the arc or to other modules. The quadrupole polarities are antisymmetric about the IP. Both types of IR modules have the same length and horizontal beam geometry as the utility module. The betatron phase advances are $3.75 \times 2\pi$ for the experimental modules. These phase advances are chosen to minimize the nonlinear chromatic effects. The two beams are separated vertically by 70 cm when entering the IRs. They are brought into collision by translating the beam trajectories toward the median plane. This is done in two steps which, combined with the 180 degree section between them, cancel each other's vertical dispersion. The two beams exchange their vertical positions after crossing the IP.

The quadrupole focusing in the IR module is strictly antisymmetric about the IP. This antisymmetry is needed to produce the same optics in both rings, since the triplet quadrupoles around the IP are shared by both beams. The antisymmetry is also the reason for including the extra half cell in the definition of the IR modules.

The small beam diameter required at the IP for collisions is obtained by having a small β^*, which in turn implies a large beta function in the adjacent triplets. For the $\beta^* = 0.5$ m module, for example, the maximum beta function in the triplet is about 8000 m. This represents a severe aperture restriction. Although acceptable for colliding beams, this aperture is too small for beam injection. Thus each IR module has an accompanying injection optics, which has much smaller maximum beta functions. Figure 6a,b shows the magnet arrangement and lattice functions of the injection optics for the two modules.

The IR module is, in the order proceeding toward the IP, composed of the following subsections [17].

3.4.1 Dispersion Suppressor

A dispersion suppressor consists of two cells, each having 3/4 the length, 2/3 the bending, and the same phase advance as a normal cell. Consequently the proper dispersion of these cells is half that of the normal cells, while the actual dispersion makes a cosine wave oscillation through the suppressor from the cell proper value at one end to zero at the other end. The shortness of these suppressors decreases the distance between interaction points. Moreover, since they have an $M = -1$ transfer matrix, they map the cell β-functions to the ends of the straight sections, providing favorable initial conditions for the IR optics.

Because of the asymmetry in the arc half-cells due to the spool pieces, the blocks of four dipoles in each suppressor half-cell must be positioned separately. These positions are reflected about the straight section centers, and are somewhat different for the suppressors in which the spools are shifted toward the nearest straight section than for those in which they are shifted away from the straight section. The suppressor half-cells are regular in total length and quadrupole length and their magnets are on the main bus.

3.4.2 Matching Quadrupole Triplet

The matching quadrupole triplet (Q4, Q5 and Q6) match the beta functions and the betatron phase advance from the dispersion suppressor to the IR triplet.

3.4.3 Vertical Translation

The vertical translation of each beam is done in two steps of 17.5 cm each. The two pairs of vertical bending magnets are located in two rather long drift spaces that have between them a section consisting of two 90-degree cells. This section has a transformation matrix $M = -1$. The vertical dispersion from the two translational steps thus cancel each other, while the beta functions outside the $M = -1$ section are unperturbed by the insert.

3.4.4 Inner Quadrupole Triplet

The quadrupole triplets (Q1, Q2, Q3) around the IP match the beta functions into the desired values at the IP. The conditions matched to are $\beta_x{}^* = \beta_y{}^* = \beta^*$ and $\alpha_x{}^* = \alpha_y{}^* = 0$, where $d\beta(s)/ds = -2\alpha(s)$. The maximum gradient of these triplet quadrupoles is 231 T/m.

The beams are injected and accelerated in the detuned optics. At the end of acceleration and necessary orbit and tune adjustments, the injection optics is gradually transformed to the low-β^* optics along a well-defined path [17]. During the change, the betatron phase advance across the module is kept fixed. The lattice functions of the collision optics are shown in Fig. 7a,b. Figure 8 shows the tuning curves for the low-β^* insertion while Fig. 9a,b shows the horizontal beta functions for this insertion during the tuning process

3.5 Utility Module

The two utility sections located side by side in the Near cluster provide space for beam injection, abort, and rf cavities. These sections are straightforward from an optics point of view. The magnet arrangement and the lattice functions are displayed in Fig. 10. The phase constraint of an IR module is applied here also; each utility module has a phase advance of $2.25 \times 2\pi$.

At each end of the utility section, there is a dispersion suppressor of the same design as that in the interaction region modules. The long non-dispersive region is convenient for beam injection and rf. Four quadrupole doublets, antisymmetrically located about the center of the section, provide the focusing. The beta functions have a peak value of about 1100 m. The aperture of these quadrupoles is larger than that of the arc quadrupoles so that there is sufficient room for the beam during injection. A 1 cm oscillation in the arcs, for example, requires 1.8 cm beam-stay-clear radius at the beta function peaks. The inner coil diameter of these quadrupoles is thus taken to be 5 cm, the same as that of the High Energy Booster quadrupoles, rather than the 4 cm used for the arc quadrupoles. The radio-frequency cavities are located in regions with lower beta functions to reduce their effects on transverse instabilities. The average beta functions in the 25 meter space for the rf cavities are $\beta_x = 220$ m and $\beta_y = 70$ m.

3.6 Optical Properties

The chromatic behaviors of the SSC for three tune conditions:

1) Collision — Two IRs with $\beta^* = 0.5$ m and two IRs with $\beta^* = 10$ m,

2) Intermediate — One IR with $\beta^* = 0.5$ m, one IR with $\beta^* = 8$ m, and two IRs with $\beta^* = 10$ m,

3) Injection — Two IRs with $\beta^* = 8$ m, and two IRs with $\beta^* = 60$ m

are shown in Figs. 11a–e. The variation of betatron tunes ν_x and ν_y and the lattice function β^* at the interaction points are shown as functions of the relative energy deviation $\delta = \Delta E/E$. This behavior is quite acceptable within the range $|\delta| < 10^{-3}$.

The momentum dependence of the beta function and its slope ($\beta' = -2\alpha$) at the interaction point will make the minimum beta function β_{min} and its location s_{min} momentum dependent

$$s_{min}(\delta) = \beta^*(\delta)\,\alpha^*(\delta)/[1 + \alpha^*(\delta)^2] \tag{3-2}$$

Over the range of beam energy spread of $\sigma_\delta = 0.5 \times 10^{-4}$ at collision energy, the value of $\alpha^*(\delta)$ is less than 0.01. The shift in the location of minimum beta function is therefore less than 0.5 cm, small compared with the rms bunch longitudinal spread of 7 cm.

The SSC is the first proton collider in which synchrotron radiation makes a noticeable impact on particle motion. The radiation damping times for the three degrees of freedom of motion are given by [6]

$$\tau_{x,y,s} = 2\,ET_0/UJ_{x,y,s} \tag{3-3}$$

where T_0 is the revolution time, U is the energy loss of a particle per revolution from

synchrotron radiation, and $J_{x,y,s}$ are the partition numbers satisfying the sum rule $J_x+J_y+J_s = 4$. For the SSC lattice and for on-momentum particles, the partition numbers are $J_x = 1\text{-}D$, $J_y = 1$, and $J_s = 2+D$, where D is of the order of $1/\nu_x^2$, or about 10^{-4}. All three damping times are thus positive, meaning particle motion is damped in all dimensions. The energy loss per turn at 20 TeV is calculated to be $U = 0.125$ MeV. Since $T_0 = 1/3585$ s, the damping time in the vertical direction is $\tau_y = 10^5$ s = 25 h.

The partition numbers are different for off-momentum particles. For the SSC lattice, the value of D changes with $\delta = \Delta E/E$ according to $dD/d\delta = 1028$. In order for both J_x and J_s to be positive, the value of D has to be between 1 and −2. This condition leads to an energy window of [18]

$$-1.94 \times 10^{-3} < \delta < 0.97 \times 10^{-3}. \tag{3-4}$$

When the energy of a particle exceeds this window, the synchrotron radiation antidamping still does not cause immediate loss of the particle since the antidamping times are very long. The partition numbers also vary, but negligibly, in the presence of orbit or dispersion errors.

3.7 Injector System

A series of accelerators are needed to present a high quality beam to the collider rings of the SSC for acceleration to 20 TeV. The use of cascaded accelerators is a now standard method of raising the energy of protons by many orders of magnitude while preserving fundamental beam parameters such as intensity and emittance. The choice of injection energy into the collider is influenced by many elements which include collider magnet field quality and aperture, correction systems, and the cost of the injector system. The consideration of these elements leads to the choice of 1 TeV as the final energy of the injector string. The layout of the injector complex is shown in Fig. 12.

3.8 Injector Parameters

The SSC injection system has been designed to satisfy the following criteria for collider operation:

3.8.1 Injection Energy of 1 TeV

The required aperture in the SSC is only weakly dependent upon the transverse emittance of the injected beam. As a result, the choice of injection energy is dictated primarily not by the beam size at injection but rather by the field quality of the collider magnets at low field. The sextupole component of the magnetic field in the dipoles due to persistent currents becomes very large at low fields. A distributed correction system that is capable of compensating for this effect in the collider has been designed and is intended. Raising the injection (i.e., minimum) energy of the collider would reduce the requirements placed upon this system. However, it would be necessary to raise the injection energy into the 2–3 TeV range ($B \approx 0.7$–1.0 T) before the system could be replaced by a lumped corrector system. The cost of this alternative in terms of the injection system is prohibitive and precludes serious consideration of such an option.

3.8.2 Filling Time of Less than 60 Minutes

The filling time of the two collider rings should clearly be small compared to both the colliding beam lifetime at 20 TeV and the single beam lifetime at injection. Since both of these lifetimes are expected to be a day or more, a filling time for the collider of a few hours would be sufficient during normal operating periods. A maximum of one hour (<30 minutes per ring) has been chosen in order to facilitate both the commissioning and diagnostic/study periods that are a necessary part of on-going operations. Shortening the filling time significantly would require a more powerful refrigeration system.

The design of the injector has been driven by two concerns, (a) the desire to guarantee preservation of transverse emittance in the presence of space charge effects at injection into the lowest energy ring and (b) the desire to avoid transition energy crossing (with the inevitable degradation of beam quality) anywhere in the system. Accommodating these two concerns restricts the injector design to be close to that described here. The injector consists of a 600 MeV (kinetic energy) linear accelerator followed by three circular accelerators. H^- ions are accelerated through a three-stage linac consisting of a radio-frequency-quadrupole front end followed by drift tube and coupled-cavity linac structures. The H^- ions are stripped at injection into a small Low Energy Booster (LEB). The LEB accelerates the protons to 8 GeV/c. The protons are transferred to the Medium Energy Booster (MEB) where they are accelerated to 100 GeV/c, and then into the High Energy Booster (HEB) where they reach the SSC injection momentum of 1 TeV/c. The LEB and MEB are both constructed with conventional magnets, while the HEB is made superconducting in order to limit its physical size. Injection into either of the two collider rings in a reasonable manner requires that the HEB be bipolar. The optics of the three rings are arranged such that the protons never cross through the transition energy of any of the rings—acceleration in the LEB occurs below transition, while acceleration in the MEB and HEB occurs above transition. Fast transverse dampers are used in all rings to minimize emittance dilution arising from injection orbit errors. All beam transfers take place in the horizontal plane and, with the exception of LEB injection, are accomplished through single turn extraction and injection.

4. Magnet Aperture and Field Quality

The critical parameter that governs the magnet aperture and field quality is the inner diameter of the superconducting coil package, designated by d_c. The magnet cost, including the costs of the superconducting material and the cryogenic system, depends sensitively on this parameter. To minimize the total magnet cost, it is desirable to have d_c as small as possible. On the other hand, the coil diameter has to be large enough to allow good field quality so that there is sufficient room for stable motion of the beam particles. In addition, the vacuum chamber pipe must fit inside the coil package with its wall sufficiently far away from the beam to avoid collective instability effects. Single particle dynamics impose the more stringent requirement and therefore set d_c. Here field quality specifications for the arc magnets are considered. For the present purposes, the interaction regions can be regarded as perfect as all of the IR magnets will be individually corrected. Also, the IR errors do not greatly contribute to the aperture when the machine is tuned for the injection optics because of the relatively small injection beta

functions. On the other hand, they dominate the aperture in the collision optics. This study is to determine the needed aperture at injection. The IR quadrupoles are included in the lattices employed in these aperture studies because they do contribute to chromatic aberrations and thus have an impact on the strengths of the chromaticity sextupoles in the arcs.

Magnet field quality specifications have been arrived at by an iterative procedure taking demonstrated magnet technology, magnetic field calculations, accelerator physics, and cost factors into consideration. The results are given and the aperture requirements and field quality specifications are self consistent.

4.1 Magnet Field Errors

The magnetic field components B_x and B_y produced by a bending magnet can be specified by a multipole expansion according to

$$B_y + iB_x = B_o \sum_{n=0}^{\infty} (b_n + ia_n)(x + iy)^n \tag{4-1}$$

where B_o is the design bending field, and x and y are the horizontal and vertical coordinates measured from the magnet center. The field errors of a magnet are specified by the multipole coefficients a_n and b_n. For a pure bending dipole magnet, a_n and b_n vanish, except for $b_o = 1$. The b_n coefficients give the normal multipole components with mid-plane symmetry while the a_n coefficients give the skewed field components. The correspondence of multipole order with the index n is that the order equals $2(n + 1)$. Thus b_2 is the normal sextupole coefficient, a_3 the skew octupole, *etc.* The dimensions of a_n and b_n are (length)$^{-n}$. It is customary to express them in units of 10^{-4} cm^{-n}, as this is the order of magnitude of the lower order coefficients in a dipole magnet of good quality. A higher order multipole coefficient of order unity in these units is potentially dangerous for particle stability. Thus one desires a magnet to have multipole coefficients that decrease reasonably rapidly with increasing n.

There are two contributions to each of the relative multipole coefficients a_n and b_n, a systematic contribution and a random contribution. The former stems from persistent-current magnetization in the superconductor, from saturation in the iron, and from conductor placement within the coil and coil placement within the iron. Persistent current effects dominate at low magnet excitation while geometric and saturation effects dominate at high excitation. The random component stems from conductor placement errors and the distribution of filament sizes and critical currents.

These various errors influence the aperture in different ways. The dynamic aperture is mainly determined by the random errors. The linear aperture (see Section 4.2.1) is influenced by both; the phase or tune part by the systematic, the amplitude part by random errors.

The systematic field errors from persistent currents have been calculated [19, 20] and checked by measurement. Errors caused by iron saturation have been calculated using the POISSON program [21] as well as measured in models [22].

4.1.1 Dipole Tolerances

The resulting specifications or tolerances for the random multipole errors of the SSC arc dipole magnets are given in Table 2, along with some results on the random errors of two sets of model magnets of the basic SSC design. The setting of these specifications has been predicated on several assumptions:

Table 2

Specifications for the rms random multipole errors in the SSC dipole magnet with $d_c = 4$ cm and 5 μm filament size. Also tabulated are rms values of the random random multipole coefficients measured on some 4.5 m BNL and 1.0 m LBL models. The units of a_n and b_n are 10^{-4}cm^{-n}.

Multipole coefficient	Specified tolerances	Measured random errors	
		BNL (6 models)	LBL (4 models)
a_1	0.7	2.77*	0.41*
a_2	0.6	0.22	0.36
a_3	0.7	0.29	0.15
a_4	0.2	0.12	0.13
a_5	0.2	0.11	0.04
a_6	0.1	0.03	0.02
a_7	0.2	0.08	0.15
a_8	0.1	0.01	0.03
b_1	0.7	0.79*	1.96*
b_2	2.0	1.24	4.27
b_3	0.3	0.15	0.27
b_4	0.7	0.30	0.68
b_5	0.1	0.03	0.08
b_6	0.2	0.06	0.14
b_7	0.2	0.05	0.16
b_8	0.1	0.01	0.10

*Coil position in yoke not adjusted to compensate.

4.1.2 Systematic Error Assumptions

(a) Systematic quadrupole distortions (a_1 and b_1) are corrected by a combination of shimming the collared coil package in the yoke and lumped correctors.

(b) Systematic sextupole (b_2) and decapole (b_4) errors from all sources are corrected by distributed windings mounted on the beam pipe inside the dipoles. Skew sextupole errors are compensated by lumped correctors.

(c) Other systematic multipoles are controlled to tolerable levels in manufacture.

4.1.3 Random Error Assumptions

(d) Random errors caused by inaccuracies in conductor placement during construction scale approximately with coil diameter d_c as [20]

$$a_n, b_n \propto d_c^{-n-\frac{1}{2}} \tag{4-2}$$

This scaling law follows from assuming that the azimuthal cable placement error scales as $r^{-1/2}$, where r is the radial position of the conductor. This scaling behavior is consistent with data from the Tevatron (700 magnets), CBA (20 magnets) and 5 cm aperture SSC prototypes (10 magnets), which have different coil diameters.

(e) The experience of manufacturing the Tevatron and CBA dipole magnets is applicable to the SSC dipoles in the estimation of reasonable tolerances on the random errors, provided the above scaling law is used to convert the earlier experience.

(f) The Tevatron experience is applicable for the estimation of the random error part of the persistent current distortions (caused by magnet-to-magnet variation in the critical current density of the superconductor and in the operating temperature).

The random error tolerances given in Table 2 are the result of three separate models of the manufacturing and component quality control tolerances, normalized to data on Tevatron and CBA magnets, and scaled according to Eq. (4-2) to d_c = 4 cm [20]. The three models, while differing in detail, yield essentially the same results for random errors expected under manufacturing and material procurement conditions achieved in the past. They are therefore a reasonable choice for the design tolerances for the arc dipoles. The random errors at low fields from persistent currents can be inferred from Tevatron data to be approximately 10% of the systematic errors from conductor variations and about 1% from temperature variations.

The model magnet program has produced enough magnets of the same types to begin to assess the degree of success in achieving the random error tolerances. The rms deviations of various multipole coefficients for a series of six 4.5 m models made at Brookhaven National Laboratory and a series of four 1.0 m models built at Lawrence Berkeley Laboratory are given in Table 2. Comparison with the specifications shows that, apart from a_1 and b_1 (which were not corrected during assembly in these models),

and some of the higher order multipoles (where measurement errors dominate the values), the measured values meet or exceed specifications.

4.1.4 Quadrupole Errors

An estimate of the rms quadrupole field error coefficients based on a scaling similar to Eq. (4-2) is given in Table 3. The effect of field errors in the normal arc quadrupoles on particle motion is small compared with that of the dipoles. On the other hand, errors of the interaction region quadrupoles do require special attention. The random error in the a_1 coefficient in Table 3 corresponds to a roll angle rms alignment error of 0.5 mrad, while that of the b_1 coefficient corresponds to rms integrated quadrupole strength error of $\Delta q/q = 5 \times 10^{-4}$.

Table 3

Estimated rms random multipole tolerances in the SSC quadrupole magnets with $d_c = 4$ cm. The units of a_n and b_n are 10^{-4} cm^{-n} with the quadrupole field evaluated at 1 cm radius.

n	1	2	3	4	5
a_n	—	2.6	1.2	0.3	0.14
b_n	—	2.9	0.5	0.3	0.56

Fringe field effects are not very important for the SSC because of the relatively great length of individual magnets. The ends of the dipole magnets are designed to minimize the multipole errors. The main effective multipole content for a dipole end is second order in the particle coordinates and is therefore equivalent to a sextupole. Its strength is found to be small compared with that of the chromaticity sextupoles. The horizontal and vertical chromaticity contributions from modeled wedge dipole fringe fields, for example, are 0 and -1.2×10^{-3}, compared with the natural chromaticities of -219.

Quadrupole fringe fields act like an octupole. Fringe fields of the interaction region quadrupoles which are strong and are located at high beta-function locations, for example, can be characterized by the horizontal and vertical tune shifts with betatron amplitudes. These values are smaller than the contribution from the rest of the unperturbed storage ring, which are in any case small.

4.2 Aperture Requirements

As mentioned before, the magnet coil size is a critical parameter for the SSC and is specified by the inner diameter of the coil package d_c. To minimize the magnet cost, d_c has to be chosen to be the minimum value allowed by particle stability considerations. To obtain the minimum d_c, it is necessary first to specify how much room is needed for the beam stability and operational purposes. This information can then be translated to the minimum value of d_c for a given cell length.

Room for particle motion in the SSC is characterized by three quantities: the linear aperture, the dynamic aperture, and the momentum aperture.

4.2.1 Linear and Dynamic Aperture

The linear aperture is a region around the axis of the magnets within which particle motion is basically linear. It represents the high quality aperture needed for routine beam operations. Within the linear aperture, not only are particle motions stable but also predictable within the approximation of linear uncoupled motion, at least for on-momentum particles. It is regarded of importance for the SSC to have sufficient linear aperture to allow for stable and efficient beam operations.

The dynamic aperture is a region larger than the linear aperture, within which particle motion is stable but not necessarily linear. If the beam is exploring the full dynamic aperture, its detailed behavior may not be easy to understand and the beam emittance may not be suitable for high luminosity runs, but it still permits valuable diagnosis, trouble shooting, and safe abort.

The linear and dynamic apertures depend differently on the magnet multipole errors. The former depends mostly on the lower order multipoles, primarily the a_2 and the b_2 errors, while the latter depends mostly on higher random multipoles. It is important that the achieved dynamic aperture be sufficiently larger than the linear aperture. It is still the linear aperture, however, that is regarded as the prime requirement in choosing the value of d_c.

Numerous particle tracking simulations have been performed, typically by tracking particles for several hundred to a few thousand revolutions. Little attempt has yet been made to study the intricate long term stability behavior of the single particle motion. This is based on the expectations that

(a) The linear aperture can be determined by a relatively small number of tracking turns. Past accelerator experience has shown that, once motion is shown to be linear, long term stability is expected.

(b) The dynamic aperture is needed for beam diagnosis and abort purposes. For these purposes, the beam need last only for several synchrotron oscillation periods, or a few thousand turns. Whether the beam has long term stability is not of prime importance.

In linear motion, the particle trajectory in phase space is a perfect ellipse and the Courant-Snyder amplitude [23] is a true invariant. When nonlinearities are present, the ellipse smears and the value of the "invariant" fluctuates from turn to turn. The rms fractional value of this fluctuation is referred to as the smear. The linear aperture is

defined quantitatively by the criteria that the maximum smear does not exceed 10% and that the on-momentum tune shift with amplitude does not exceed 0.005. The linear aperture is given by the amplitude beyond which either one of the two criteria is violated. This definition is based on past accelerator experience [24]. Further accelerator studies, at the Tevatron, to improve the accuracy of these criteria are currently underway.

4.2.2 Needed Linear Aperture

The needed linear aperture is a function of lattice cell design, particularly the half-cell length L and the betatron phase advance per cell μ. In the following, μ is fixed to be 90 degrees while the aperture dependence on L is studied.

The aperture required is largest at injection and is composed of several components. For a location with a typical beta function of 388 m, these requirements are [25]

(a) Beam size — for a typical half-cell length L = 114 m, the beam size is $\sqrt{6}\sigma$ = 1.5 mm at 1 TeV and 0.33 mm at 20 TeV.

(b) Beam position fluctuation at injection — up to 1.5 mm.

(c) Orbit distortions — up to 1.25 mm.

(d) Miscellaneous effects (power supply ripple, lattice mismatch, etc.) — up to 0.5 mm.

These aperture requirements can be scaled to different half-cell lengths. An empirical expression for the needed linear aperture (expressed as a transverse amplitude), valid approximately in the range L = 50 m to 150 m, is [16]

$$A_{\text{linear}}\,(\text{mm}) = 0.692\,[L\,(\text{m})]^{0.41} \tag{4-3}$$

For example, with L = 114 m, Eq. (4-3) gives a linear aperture requirement of 4.8 mm. The aperture requirements relax substantially after injection. The needed aperture does not depend sensitively on the injection energy because the beam size is not a dominating contribution to the aperture need.

The aperture required because of injection errors can be reduced substantially by applying a feedback system to damp the betatron and energy oscillations rapidly. In the aperture requirement, Eq. (4-3), however, this is not taken into account.

Having defined the required aperture for beam stability and operation, it is necessary to specify the field quality that achieves this requirement. The field quality, as mentioned before, is governed mainly by the magnet coil size d_c. The random error coefficients a_1 and b_1, not included here, produce linear distortions that must be controlled by quadrupole and skew quadrupole correction elements.

It is possible to improve the linear aperture substantially by "binning" the magnets [26]. The multipoles of all magnets will be measured. The magnets can then be connected to one of a few different correction power supplies for a given multipole. For instance, in order to correct the b_2 coefficients of the magnets, the measured sextupole errors could be histogrammed into seven bins and a separate correction power supply could be assigned to each bin. Each magnet would then be attached to the supply for its bin. When this simple binning is applied, the effective rms variation of the random

sextupole moment is found to be reduced by a factor of five [16]. Binning is clearly an effective means to improve the aperture [17].

For given d_c and L, analytical and numerical techniques can be applied to calculate the achieved linear aperture. Tools used in the numerical studies consists of several particle tracking programs including DIMAT [28], PATRICIA [29], MARYLIE [30], RACETRACK [31] and TEAPOT [32]. The motions of single particles with various betatron amplitudes and momentum offsets are tracked in the presence of magnet field errors (omitting a_1 and b_1) to determine the smear and the tune shifts. An empherical fit to the tracking results on linear aperture [16] can be summarized by the expression

$$A_{\text{linear}}(\text{mm}) = (19 \pm 2)\,[L\,(\text{m})]^{-0.45}\,[d_c\,(\text{cm})]^{1.1} \tag{4-4}$$

The region of applicability for Eq. (4-4) is approximately L = 50 to 150 m and d_c = 2.5 to 5 cm. The achieved aperture depends on the specific values and distribution of the random field errors. The rms deviation in Eq. (4-4) reflects the rms spreads in the random magnet errors and binning on the random sextupole moment in seven bins. For L = 114 m and d_c = 4 cm, the achieved aperture is (10.3 ± 1.1) mm, compared with the needed aperture of 4.8 mm.

4.2.3 Dynamic Aperture

Dynamic aperture, like the linear aperture, is obtained by tracking particles with various starting betatron amplitudes. The maximum amplitude that allows stable motion for typically 400 revolutions is identified as the dynamic aperture. Instability is identified when the particle amplitude exceeds a cut-off which is typically taken to be 1 m. Tests are made to show that the dynamic aperture so obtained does not change appreciably with the number of revolutions tracked and the amplitude cut-off. Tracking studies have shown that the achieved dynamic aperture is about 70% larger than the achieved linear aperture.

4.2.4 Momentum Aperture

In addition to the on-momentum linear and dynamic apertures, we must consider their momentum dependences. For beam stability and operation, it is necessary to provide sufficient room for not only the on-momentum particles but also the off-momentum particles. The momentum aperture refers to the range of energy deviation within which the linear and the dynamic apertures are substantially maintained. The momentum aperture requirements should cover the injection energy errors ($<1.5 \times 10^{-4}$) and the fractional beam energy spread at injection of $\sqrt{6}\,\sigma_\delta = 4.6 \times 10^{-4}$. It is suggested that, for the SSC, an aperture of $\Delta E/E = \pm 10^{-3}$ should be sufficient to accommodate these requirements. The energy spread of the beam and consequent rf specification are determined by the need to counteract certain collective instabilities.

To explore the momentum aperture, off-momentum particles with given $\Delta E/E$ are tracked for typically 400 revolutions and the dynamic aperture is obtained for each momentum. The momentum aperture is then indicated by the momentum deviation beyond which the dynamic aperture is substantially reduced from the on-momentum value. Off-momentum dynamic aperture has also been evaluated when the random linear

field errors a_1 and b_1 are included. Using TEAPOT, the results with five sets of random numbers are:

δ	Without binning	With binning
−0.001	7.7 ± 1.6 mm	11.1 ± 0.5 mm
0.0	10.1 ± 1.3	13.5 ± 2.4
+0.001	9.8 ± 2.7	13.0 ± 0.5

The linear distortions have been corrected by four families of skew quadrupoles. Sorting here was made mainly on the b_2 coefficients but also on a_1. The off-momentum dynamic aperture has not decreased because of the linear field errors. Tracking studies are also used to find the off-momentum linear aperture. The results show a decrease of a factor of two from the on-momentum value at $\delta = \pm 10^{-3}$. The reduction of linear aperture off-momentum is somewhat more than that of the dynamic aperture because of the feeddown of higher multipoles, but the factor of two reduction at $\delta = \pm 10^{-3}$ is believed acceptable [33].

5. Collider Operational Consideration

Proton beams are prepared in the High Energy Booster and injected into the collider rings at 1 TeV. Section 5.1 describes injection and the acceleration cycle in the collider rings. During this stage, beams are separated at the interaction points to avoid beam-beam effects. A beam executes betatron or synchrotron oscillations when injected with error. These oscillations need to be damped by feedback systems.

The magnet strengths, the rf voltage and rf frequency are controlled in synchronism during the 1000 seconds of acceleration. Several beam parameters, such as beam size, bunch length, energy spread and synchrotron tune, vary accordingly in synchronism along the path. These variations are discussed in Section 5.1.

In the SSC, several processes contribute to particle loss and phase-space dilution. It is customary to describe the particle loss rate by a beam lifetime. Similarly, particle loss and phase-space dilution contribute to a luminosity lifetime. In detail, however, the behaviors of both the beam intensity and the luminosity with time during storage are not simple exponentials. In particular, synchrotron radiation damping makes the beam emittance shrink. Shrinking emittance in turn makes the luminosity increase, which causes a higher rate of particle loss. Shrinking emittance also makes the intrabeam scattering stronger, retarding further emittance shrinking. The interplay among the beam intensity, the luminosity, the emittance and other parameters is described in Section 5.2.

5.1 Injection and Acceleration Cycle

Each collider ring is filled with fifteen beam batches from the 1-TeV High Energy Booster (HEB). Each batch is 17.5 μs in length (1092 bunches) and is loaded 0.15 μs behind its predecessor batch. With the revolution time of 276.7 μs, this arrangement produces a 3.1-μs abort gap between the first and the last batches. The injection-kicker rise time must be less than 0.15 μs, but its fall time can be as long as 3.1 μs. The 60-second cycle time of the HEB allows the 15 batches to be loaded in 15 minutes.

After one collider ring is filled, the polarity of the HEB is reversed and its injection and extraction systems switched so as to be able to load the second collider ring in the opposite direction. The polarity change may take a few minutes. Both rings may thus be loaded in approximately 35 to 40 minutes, allowing for several low-intensity test pulses to be made prior to the actual loading process.

5.1.1 Beam Injection

Beam-beam collisions are avoided by separating the beams near the crossing regions during injection and the acceleration ramp. In both cases, the beams are separated horizontally by 4 mm at the interaction point and injected with a vertical opening angle (40 μrad for the intermediate-luminosity case and 90 μrad for the high-luminosity case) in order to maintain a beam-beam separation of at least 10 local beam-size standard deviations throughout the region between the vertical splitting magnets (332 m and 159 m in the two cases). After acceleration to 20 TeV, the beams are moved horizontally into collision and the crossing angle is set to 75 μrad. The crossings can be either horizontal or vertical. As the beams are brought into collision, a slight orbit adjustment at the interaction point can be performed to compensate for the orbit distortion caused by the long-range beam-beam interaction. These corrector settings can be predetermined.

For injection, the optics of the four interaction regions are modified so as to require less aperture in the high-β regions and to be more tolerant of small injection errors. After injection and acceleration, the optics are gradually transformed into the collision optics along a carefully chosen path [17].

To ensure beam stability at injection against single-bunch transverse effects, the longitudinal emittance $\varepsilon_s = \sigma_E \sigma_t$ will be increased from 0.0016 eV-s to 0.035 eV-s in the HEB before injection into the collider.

5.1.2 Feedback Systems for Injection Errors

Collective betatron oscillations result from inevitable injection errors. Feedback systems of strength sufficient to damp them before significant emittance growth occurs are provided. This feedback process, taking into account the random magnetic field errors and magnet sorting has been simulated by particle tracking [34]. The strengths of the horizontal and vertical damping systems are capable of giving a ±2 μrad kick per cm of displacement, if located at points of normal beta. At 1 TeV, this corresponds to a damping time of 45 revolutions. The injected beam has normalized emittances of $\varepsilon_x = \varepsilon_y = 1$ μm-rad, and an rms relative energy spread of $\sigma_\delta = 1.5 \times 10^{-4}$. In the simulation it was assumed that the chromaticities from random sextupoles have been corrected by adjusting the chromaticity sextupoles. Injection jitter tolerances have been set to be ±1.5

mm in x and y and $\pm 1.5 \times 10^{-4}$ in δ [25]. Without feedback, the beam size would double by filamentation, but the feedback system is capable of preserving the beam sizes under these injection errors. Beams injected with much larger errors (for example, because of failure of one of the injector kicker modules) will suffer significant beam size growth, and have to be aborted for colliding beam operations. It is envisioned that the feedback system also serves to control the collective instabilities.

5.1.3 Orbit, Chromaticity, and Persistent Current Correctors

Two other correction systems are normally active throughout the operating cycle. Dipole coils in the correction spools serve to correct the horizontal and vertical closed orbits and sextupole coils in the spools reduce the normal chromaticity to approximately zero. These correction systems track the ring magnets. A separate correction system will be used to compensate the magnetic field perturbations due to the persistent currents in the superconducting filaments and saturation in the iron. The sextupole and decapole components of these known field errors are corrected by coils distributed on the dipole bore tubes. These corrections are maintained during injection and acceleration.

5.1.4 Acceleration Cycle

The two beams are accelerated from 1 to 20 TeV in 1000 seconds. It is necessary that several collider parameters be changed in a programmed manner during acceleration. The magnets are ramped linearly in time, requiring an energy gain of 5.26 MeV per turn. To stabilize transverse and longitudinal emittance growth from intrabeam scattering during the storage cycle, the longitudinal emittance is increased approximately linearly with time during the acceleration cycle from 0.035 to 0.233 eV-s by controlled injection of rf noise into the 354 MHz acceleration system. A constant peak rf voltage of 20 MV is satisfactory for this acceleration cycle. Figure 13a,b gives the values of several parameters during the 1000-second acceleration time. Feedback control of beam stability along the path has been verified using the program ZAP [35, 36].

5.2 Beam and Luminosity Lifetimes

Table 4 lists several processes of particle loss and emittance change, together with their underlying causes. In this section, we discuss the effect of these processes on the beam intensity and the luminosity. Collective effects, effects of magnet field nonlinearities and beam-beam effects are not treated. Proper choices of operating conditions and corrections make these latter effects unimportant in the present considerations.

Table 4

Leading Causes of Particle Loss and Emittance Change in the SSC

Causes	Particle Loss	Emittance Change
beam collisions at interaction points	inelastic interactions	elastic scattering
residual gas	nuclear interaction	multiple scattering
Coulomb scattering within bunch	Touschek lifetime (single scattering)	intrabeam scattering (multiple scattering)
synchrotron radiation	quantum lifetime (effect negligible)	radiation damping

Ignoring the small modification introduced by a finite crossing angle, the rate of change of luminosity $\mathcal{L}$ is related to the rates of change of the number of particles per bunch N_B and the emittance ε through

$$\frac{1}{\mathcal{L}}\frac{d\mathcal{L}}{dt} = \frac{2}{N_B}\frac{dN_B}{dt} - \frac{1}{\varepsilon}\frac{d\varepsilon}{dt} \tag{5-1}$$

The particle loss rate per bunch from proton-proton collisions is given by

$$(dN_B/dt)_{\mathrm{pp}} = -\mathcal{L}_t \Sigma_{\mathrm{inel}}/M \tag{5-2}$$

where $\mathcal{L}_t$ is the total luminosity at two IRs with $\beta^* = 0.5$ m and two IRs with $\beta^* = 10$ m, $\Sigma_{\mathrm{inel}} = 90$ mb is the cross section for inelastic collisions, $M = 15456$ is the number of bunches per beam. The initial loss rate, Eq. (5-2), is 1.1×10^4 particles/s per bunch. Another possible contribution to particle loss collisions is bremsstrahlung. It is estimated that, for the SSC with two high-luminosity IRs, the loss rate is only about 40 protons/s [37].

Although the main particle loss is from collisions in the IRs, other processes contribute. The second particle loss mechanism listed in Table 4, residual gas nuclear scattering, is given by

$$\begin{aligned}\frac{1}{N_B}\frac{dN_B}{dt} &= -c\sum_i N_i\sigma_i \\ &= -\sum_i \frac{(P_i/10^{-9}\,\mathrm{Torr})(\sigma_i/52\mathrm{mb})}{5030\,\mathrm{h}}\end{aligned} \tag{5-3}$$

where N_i is the number density of the ith molecular species in the gas, σ_i the cross section for a 20 TeV proton incident on the ith kind of molecule, and P_i is the room-temperature-equivalent partial pressure of the ith species. The partial pressures are estimated on the basis of desorption measurements made at the National Synchrotron Light Source [38]. From them we obtain a residual gas nuclear scattering lifetime of

greater than 300 h, or an initial particle loss rate of 7000 s^{-1} per bunch. This particle loss contributes a cryogenic load of 380 watts per beam.

The third mechanism is the Touschek effect [39]. The loss rate is

$$(dN_B/dt)_{\text{Touschek}} = -(9.4\times10^{-19}\ \text{s}^{-1})\, N_B^2 \tag{5-5}$$

which gives a negligible initial loss rate of 53 particles per second per bunch.

Similarly, the emittance change has contributions from the four mechanisms listed in Table 4. The first contribution from elastic collision events can be written as

$$(d\varepsilon/dt)_{\text{pp}} = (\beta_1{}^*\,\mathcal{L}_1 + \beta_2{}^*\,\mathcal{L}_2)\sigma_{\text{el}}\langle\theta^2\rangle/MN_B \tag{5-6}$$

where $\langle\theta^2\rangle^{1/2} = 9$ μrad is the estimated rms projected scattering angle at 20 TeV [40], $\sigma_{\text{el}} = 30$ mb is the estimated elastic scattering cross section, $\beta_{1,2}{}^*$ and $\mathcal{L}_{1,2}$ are the beta-functions and luminosities of the two high-luminosity and two intermediate-luminosity interaction points, respectively. Taking $\beta_1{}^* = 0.5$ m, $\beta_2{}^* = 10$ m and initial values of $\mathcal{L}_1 = 10^{33}\ \text{cm}^{-2}\text{s}^{-1}$ and $\mathcal{L}_2 = 5.6\times10^{31}\ \text{cm}^{-2}\text{s}^{-1}$, we obtain an initial rate of $(d\varepsilon/dt)_{\text{pp}} = 2.0\times10^{-17}$ m/s.

Multiple scattering from the residual gas contributes

$$(d\varepsilon/dt)_{\text{RG}} = c\,\beta_{\text{ave}}\, d\langle\theta^2\rangle/ds \tag{5-7}$$

This can be rewritten as

$$(d\varepsilon/dt)_{\text{RG}} = (1.76\times10^3\ \text{m s}^{-1})\,\beta_{\text{ave}}\left[\frac{14.1\ \text{MeV/c}}{p_o}\right]^2 \sum_i \frac{P_i\mu_i}{X_i} \tag{5-8}$$

where p_o is the beam momentum and P_i, μ_i, and X_i are, respectively, the partial pressure (in Torr), molecular weight (in g/mole), and the radiation length (in g cm^{-2}) for the ith molecular species in the residual gas. Using the known composition and limits, one obtains $(d\varepsilon/dt)_{\text{RG}} < 7\times10^{-17}\ \text{m s}^{-1}$.

The remaining two effects on emittance changes are the most important for the SSC. The result of intrabeam scattering at 20 TeV can be summarized by the approximate expression

$$(d\varepsilon/dt)_{\text{IBS}} = 3.3\times10^{-37} N_B/\varepsilon \tag{5-9}$$

With $N_B = 8.0\times10^9$ and $\varepsilon = 4.7\times10^{-11}$ m, the initial emittance growth rate is $(d\varepsilon/dt)_{\text{IBS}} = 5.6\times10^{-17}$ m/s. Although this initial rate is only comparable to the two previous effects, the intrabeam scattering contribution becomes more important as the emittance shrinks by synchrotron radiation damping.

Synchrotron radiation damping times are 12.4 hours and 24.8 hours for the longitudinal and transverse amplitudes respectively. The transverse emittance damping time is half that of the amplitude damping time, or 12.4 hours. This gives

$$(d\varepsilon/dt)_{\text{SR}} = -1.04\times10^{-15}\ \text{m/s}\ . \tag{5-10}$$

The initial rates of change of N_B and ε produce an increasing luminosity; however, they are not sufficient to determine the long-term behavior of the beam intensity and the luminosity. The interplay among the parameters N_B, $\mathcal{L}_t$ and ε are obtained by numerically integrating the rate equations. With these parameters given, the head-on and long-range beam-beam tune shifts, $\Delta\nu_{HO}$ and $\Delta\nu_{LR}$, can be obtained as functions of time. These results are shown in Fig. 14a,b.

Because of synchrotron radiation damping, the luminosity increases initially as the emittance decreases with time. For small emittances, intrabeam scattering becomes more important, slowing the emittance damping process. In the meantime, the beam intensity decreases sufficiently that the luminosity reaches a maximum and then decreases with time. After 50 hours of colliding beams, the luminosity is still roughly 10^{33} $cm^{-2}s^{-1}$. In this scenario, we have not restricted the number of events per collision. In case this constitutes a problem for the detectors, it is conceivable that β^* can be increased by small steps to compensate for the increasing luminosity. It is possible that, in steady state of operation, the beams can be kept colliding for a few days before a refill is needed.

6. Experiments at the SSC

The primary goal of the SSC is to allow the search for new phenomena which may be present at the TeV mass scale or below [2]. Such phenomena may include, for example, the production of new quarks or leptons, new families of particles (such as supersymmetric particles) or manifestations of structure within quarks, heretofore believed to be point-like particles. In addition, the SSC will be the most copious source to date of many known particles, allowing the study of rare decay modes not accessible at other accelerators. Also of interest will be the study of the behavior of "ordinary" proton-proton collisions in an energy region not yet explored.

Although a large number of workshops and summer studies have been devoted to exploration of the physics possibilities at the SSC and to the concomitant detector requirements, at the present time the experimental program for the SSC has not been formulated [41]. Nevertheless it is possible to classify potential experiments into four rough categories:

(1) large 4π detectors designed to operate at or very near the maximum design luminosity;

(2) spectrometers to detect rare decay modes of known particles, particularly mesons containing the b quark;

(3) experiments aimed at exploration of the basics of the copious pp collisions, such as total cross section measurements, intrajet properties, multiplicities and many more;

(4) and specialized experiments to detect truly exotic phenomena, such as magnetic monopoles, that might be overlooked by the other devices. Within each of these rough categories there are many different possibilities. Different 4π detectors, for example, will emphasize different aspects of detecting the particles produced in rare high transverse momentum pp collisions which may result in new phenomena.

A typical 4π detector for the SSC will be very similar in concept to those now existing or being built for experiments at colliding beam facilities around the world. Such detectors for the SSC, however, will be larger and significantly more complex. An example is given in Fig. 15. This example weighs approximately 50,000 tons and has about one million channels of electronics. Constructed in the usual layered fashion, 4π detectors for the SSC may contain:

- vertex detectors to accurately located secondary vertices
- high precision tracking devices to track individual particles, perhaps over a limited solid angle
- relatively low precision tracking devices to tracking isolated particles such as electrons or muons
- a magnetic field to bend the particles and hence determine the momentum
- precision electromagnetic and hadronic calorimetry covering the maximum feasible solid angle
- magnetized iron for detection of muons and measurement of their momenta

A major challenge in such detectors will be the ability to select a few events per second to record permanently for later analysis from the 100 million pp collisions which will occur every second at the design luminosity.

Another class of detector is represented by the forward spectrometer shown in Fig. 16. The primary aim of this device is to detect the decay of B mesons and thereby to search for rare decay modes and CP violation. Spectrometers such as this are similar in concept to fixed target experiments at Fermilab or CERN. They contain precision vertex detectors to tag the presence of the relatively long-lived B mesons, tracking chambers and magnets to measure momenta, calorimeters to detect electrons and photons, ring imaging Cerenkov counters to identify pions, kaons and protons and muon detection consisting of iron absorber and tracking detectors. The increase spaced between interaction region quadrupoles required for these spectrometers results in operation at reduced luminosity, about a factor of 10–20 below the maximum. Even so, tens of thousands of B mesons will be produced each second and it will be a formidable task to select out the decays on interest for storage on magnetic tape or other media.

Many other experiments are possible at the SSC, ranging from measurements of proton-proton elastic scattering to searches for massive, long-lived new particles. These experiments typically require much less apparatus and running time than 4π detectors or rare decay spectrometers. As a result they do not require dedication of an interaction region for many years as do the more massive and costly detectors. Hence, the initial experimental program at the SSC will likely consist of a mix of a few 4π detectors and large forward spectrometers and a number of smaller and quicker experiments designed to measure specific properties of the pp collisions or search for exotic phenomena.

Acknowledgements

The author would like to gratefully acknowledge the essential help of A. Chao, G. Gilchriese, and K. Metropolis in preparing this report.

References

1. SSC Conceptual Design Report, SSC Central Design Group Report No. SSC-SR-2020 (1986).
2. E. Eichten, I. Hinchliffe, K. Lane and C. Quigg, Rev. Mod. Phys. **56**, 579(1984).
3. F. Amman and D. Ritson, *Proc. Int. Conf. on High Energy Accelerators*, Brookhaven National Laboratory (1961), p. 262.
4. L. Evans and J. Gareyte, IEEE Trans. Nucl. Sci. **NS-32**, 2234 (1985).
5. P.L. Morton and J.F. Schonfeld, in Proc. Workshop on Accelerator Physics Issues for a Superconducting Super Collider, Ann Arbor, Michigan, ed. M. Tigner, University of Michigan report UM HE 84-1 (1984), p. 54–5.
6. M. Sands, in *Physics with Intersecting Storage Rings*, Proc. Int. School of Phys. "Enrico Fermi", Varenna, Course 46, ed. B. Touschek, Academic Press, NY (1971), p. 257.
7. J.M. Peterson and D.E. Johnson, SSC Central Design Group Internal Report No. SSC-N-449 (1987).
8. D.E. Johnson, SSC Central Design Group Internal Report No. SSC-N-151 (1986).
9. Report of the Reference Designs Study Group on the Superconducting Super Collider, U.S. Department of Energy (May 8, 1984).
10. Realistic Lattices Group, SSC Central Design Group Report No. SSC-SR-1015 (1985).
11. Task Force on Commissioning and Operations, SSC Central Design Group Report No. SSC-SR-1005 (1985).
12. Clustered IR Study Group, SSC Central Design Group Report No. SSC-SR-1014 (1985).
13. B. Leemann and A. Wrulich, SSC Central Design Group Internal Report No. SSC-N-133 (1986).
14. D. Neuffer, Appendix, SSC Central Design Group Report No. SSC-2 (1984), submitted to Part. Accel., 1985.
15. B. Montague, private communication (1986). For an example of clustered IR design with a (3,3) arrangement, see D. Blechschmidt et al., Nucl. Inst. Methods **156**, 375 (1978). IR pairing was considered for LEP. Note that the range of δ for LEP is 10 times that of the SSC.
16. Cell Lattice Study Group, SSC Central Design Group Report No. SSC-SR-1024 (1986).
17. A.A. Garren and D.E. Johnson, SSC Central Design Group Report No. SSC-146 (1987).
18. S. Peggs, SSC Central Design Group Internal Report No. SSC-N-130 (1986).
19. M.A. Green, in *Workshop on Accelerator Physics Issues for a Superconducting Super Collider*, Ann Arbor, Michigan, December 1983, ed. M. Tigner, University of Michigan Report No. UM HE 84-1, p. 126.

20. H.E. Fisk et al., SSC Central Design Group Report No. SSC-7 (1985).
21. POISSON, developed by K. Halbach and R. Holsinger, is a descendant of the TRIM program, A. Winslow, J. Comp. Phys. **1**, 149 (1967).
22. See, for example, P. Dahl et al., Brookhaven National Laboratory Report No. BNL-37011 (1985), in Proc. 9th Int. Conf. on Magnet Technology, Zurich, September 1985 (to be published).
23. E.D. Courant and H.S. Snyder, Ann. Phys. **3**, 1 (1958).
24. D. Edwards, SSC Central Design Group Report No. SSC-22 (1985). T.L. Collins, SSC Central Design Group Report No. SSC-26 (1985).
25. M. Harrison, SSC Central Design Group Report No. SSC-27 (1985).
26. R. Talman, SSC Central Design Group Internal Report No. SSC-N-192 (1986).
27. Aperture Task Force, SSC Central Design Group Report No. SSC-SR-1013 (1985).
28. R.V. Servranckx and K.L. Brown, Stanford Linear Accelerator Center Report No. SLAC-270 (1984).
29. H. Wiedemann, Stanford Linear Accelerator Center Internal Report No. PEP-220 (1976).
30. A. Dragt, in *Physics of High Energy Particle Accelerators*, A.I.P. Conf. Proc. No. 87, ed. R.A. Carrigan, F.R. Huson, and M. Month, American Institute of Physics, NY (1982), p. 147.
31. A. Wrulich, DESY Report No. DESY 84/26 (1984).
32. L. Schachinger and R. Talman, SSC Central Design Group Report No. SSC-52 (1985).
33. E. Forest and A. Wrulich, SSC Central Design Group Internal Report No. SSC-N-44 (1985).
34. D.E. Johnson, SSC Central Design Group Report No. SSC-60 (1986).
35. S. Chattopadhyay, SSC Central Design Group Internal Report No. SSC-N-152 (1986).
36. M. Zisman, S. Chattopadhyay, and J.J. Bisognano, Lawrence Berkeley Laboratory Report No. LBL-21270 (1986).
37. A. Chao and J.D. Jackson, SSC Central Design Group Internal Report No. SSC-N-86 (1985).
38. H. Jostlein et al., submitted to J. Vac. Sci. Technol. (1986).
39. C. Bernardini et al., Phys. Rev. Lett. **10**, 407 (1963).
40. Clustered Interaction Study Group, SSC Central Design Group Report No. SSC-SR-1014 (September 1985), p. 30.

41. For studies of SSC physics and detectors see, for example the Proceedings of the 1984 Summer Study on the Design and Utilization of the Superconducting Super Collider, Rene Donaldson and Jorge Morfin, eds., Snowmass Colorado; the Proceedings of the 1986 Summer Study of the Physics of the Superconducting Super Collider, Rene Donaldson and Jay Marx, eds., Snowmass, Colorado, 1986; and the Proceedings of the Workshop on Experiments, Detectors and Experimental Areas for the Supercollider, Rene Donaldson and M. Gilchriese, eds., Berkeley, California 1987, World Scientific to be published.

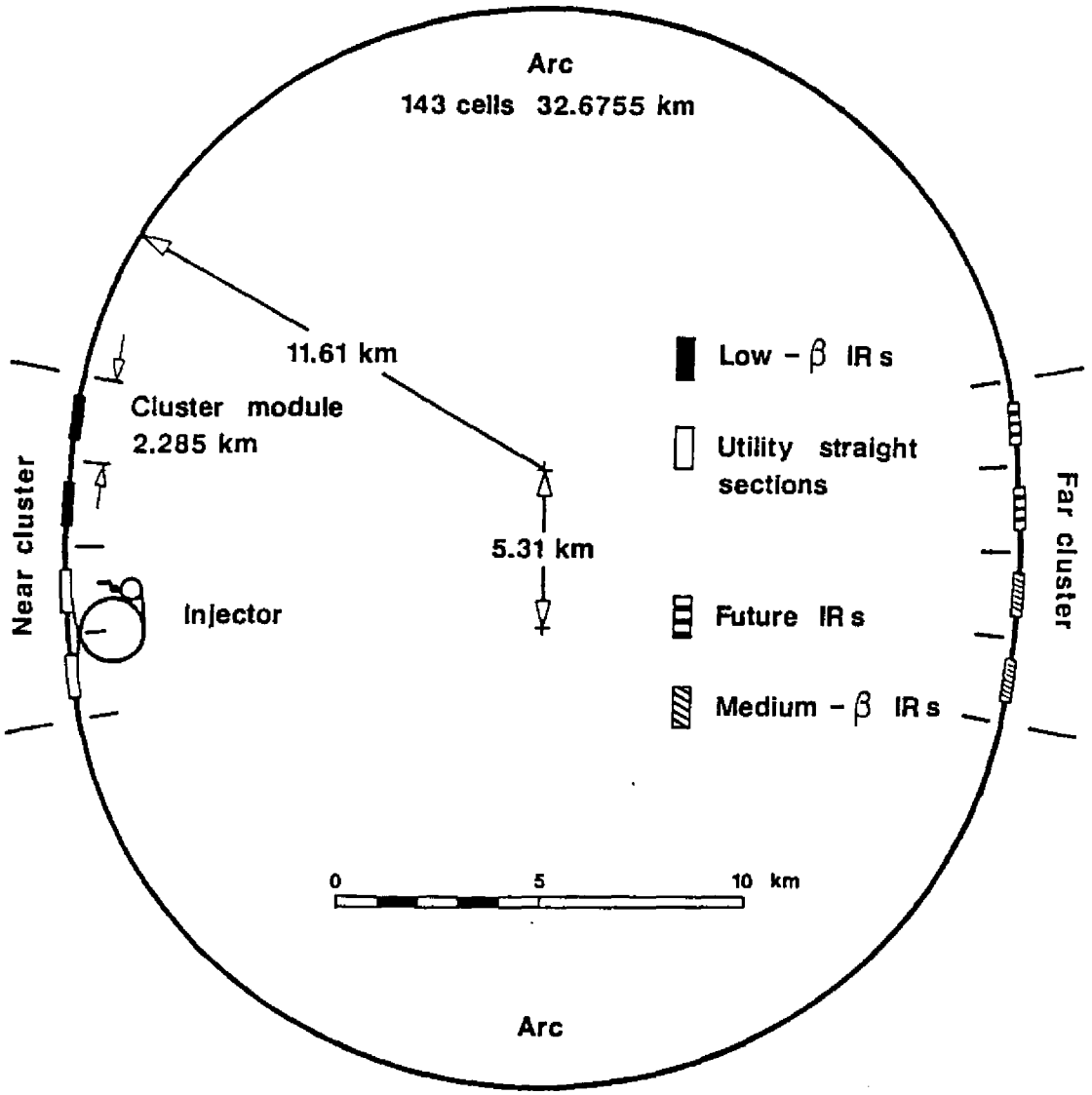

Fig. 1. SSC Ring Layout.

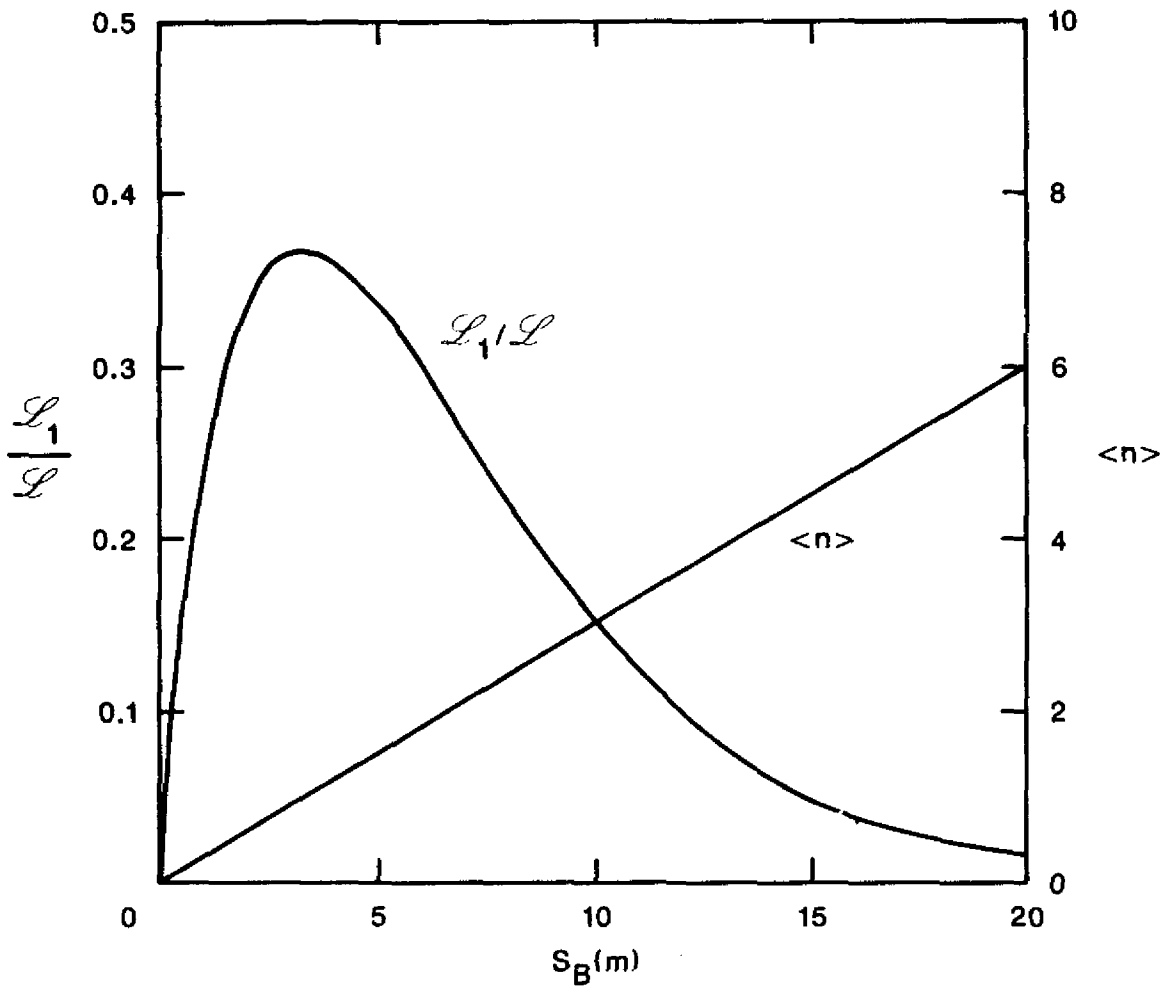

Fig. 2. The average number of interactions per bunch crossing, $\langle n \rangle$, and the single-event luminosity relative to the total luminosity, $\mathcal{L}_1/\mathcal{L}$, as functions of bunch spacing S_B in meters.

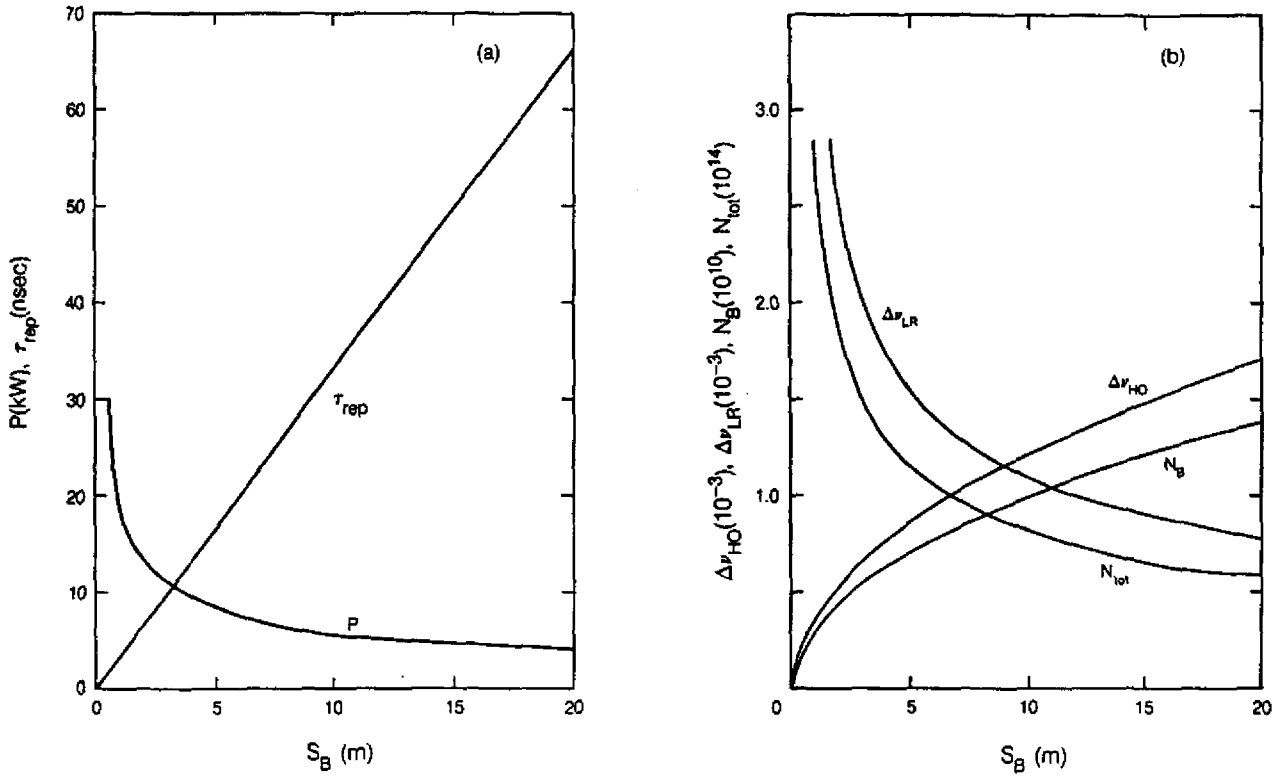

Fig. 3. Dependence of various primary parameters on the bunch spacing S_B. (a) the synchrotron radiation power P and the detector repetition time τ_{rep}, versus S_B. (b) the head-on and long-range beam-beam tune shifts $\Delta\nu_{HO}$ and $\Delta\nu_{LR}$, number of particles per bunch N_B, and total number of particles per beam N_T versus S_B.

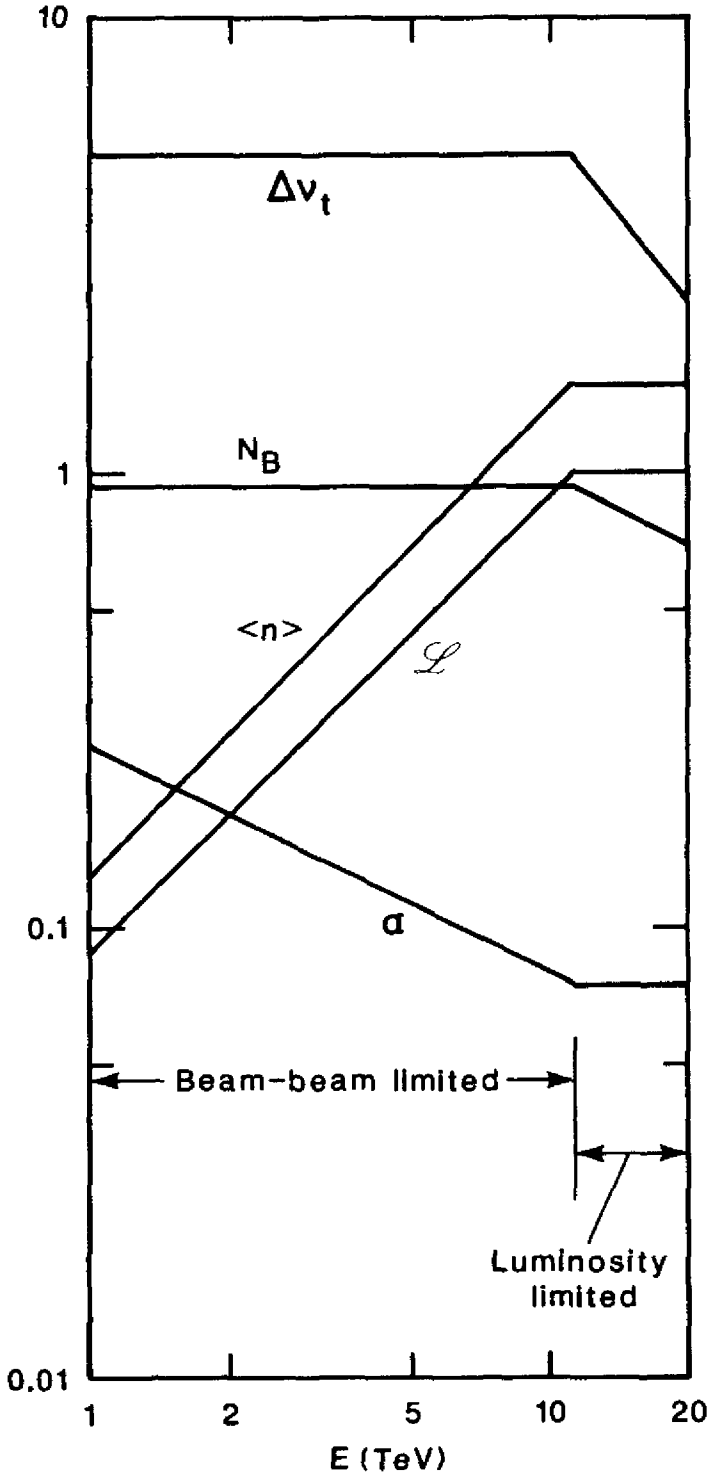

Fig. 4. Dependence of a few primary parameters on the beam energy. In this scenario, the operation is luminosity limited above 11.2 TeV and beam-beam limited below 11.2 TeV. The units for the parameters are $[\mathcal{L}] = 10^{33}$ cm^{-2} s^{-1}, $[\alpha]$ = mrad, $[\Delta\nu_t] = 10^{-3}$ and $[N_B] = 10^{10}$.

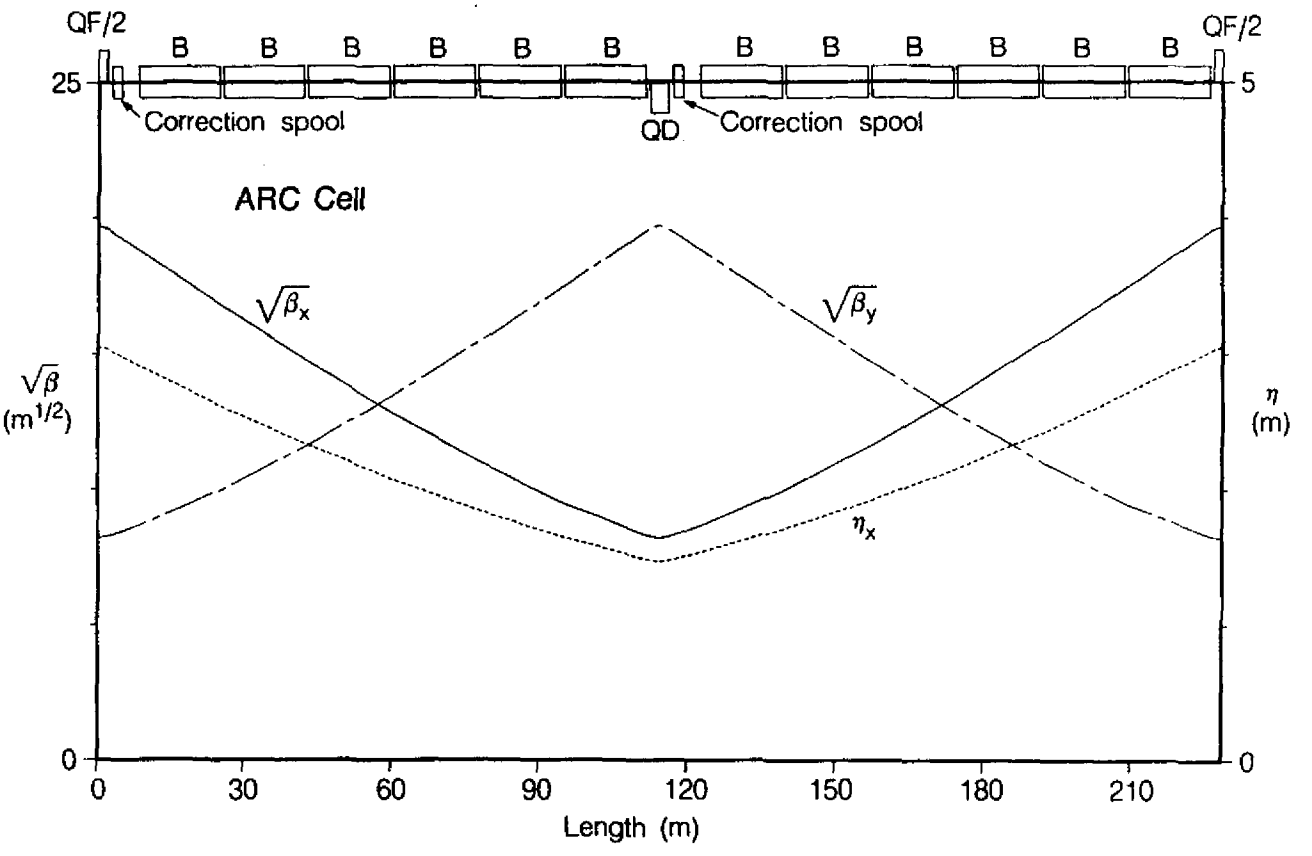

Fig. 5. Lattice and β-functions of arc cell.

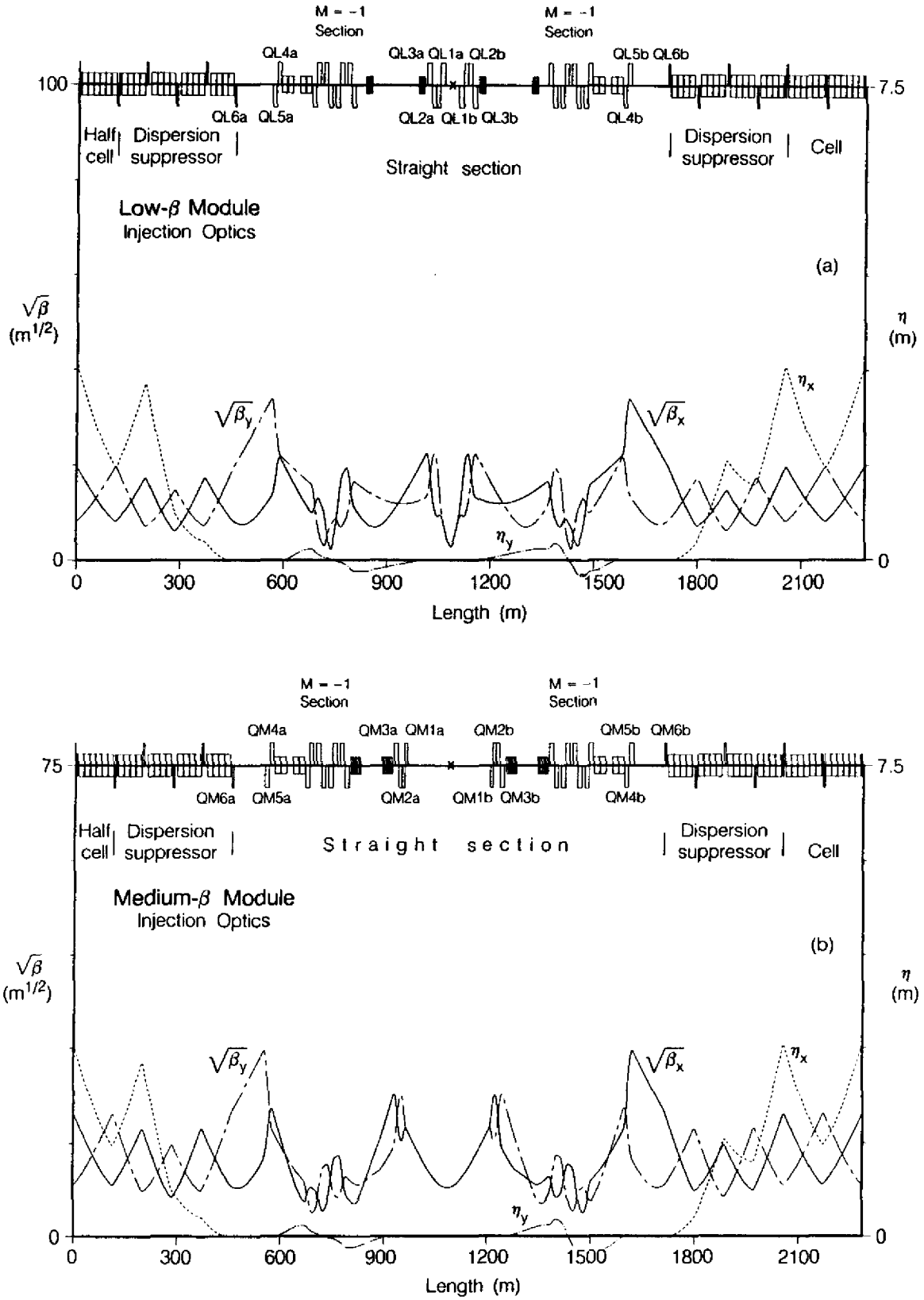

Fig. 6. (a) Low-β module; injection optics. (b) Medium-β module; injection optics.

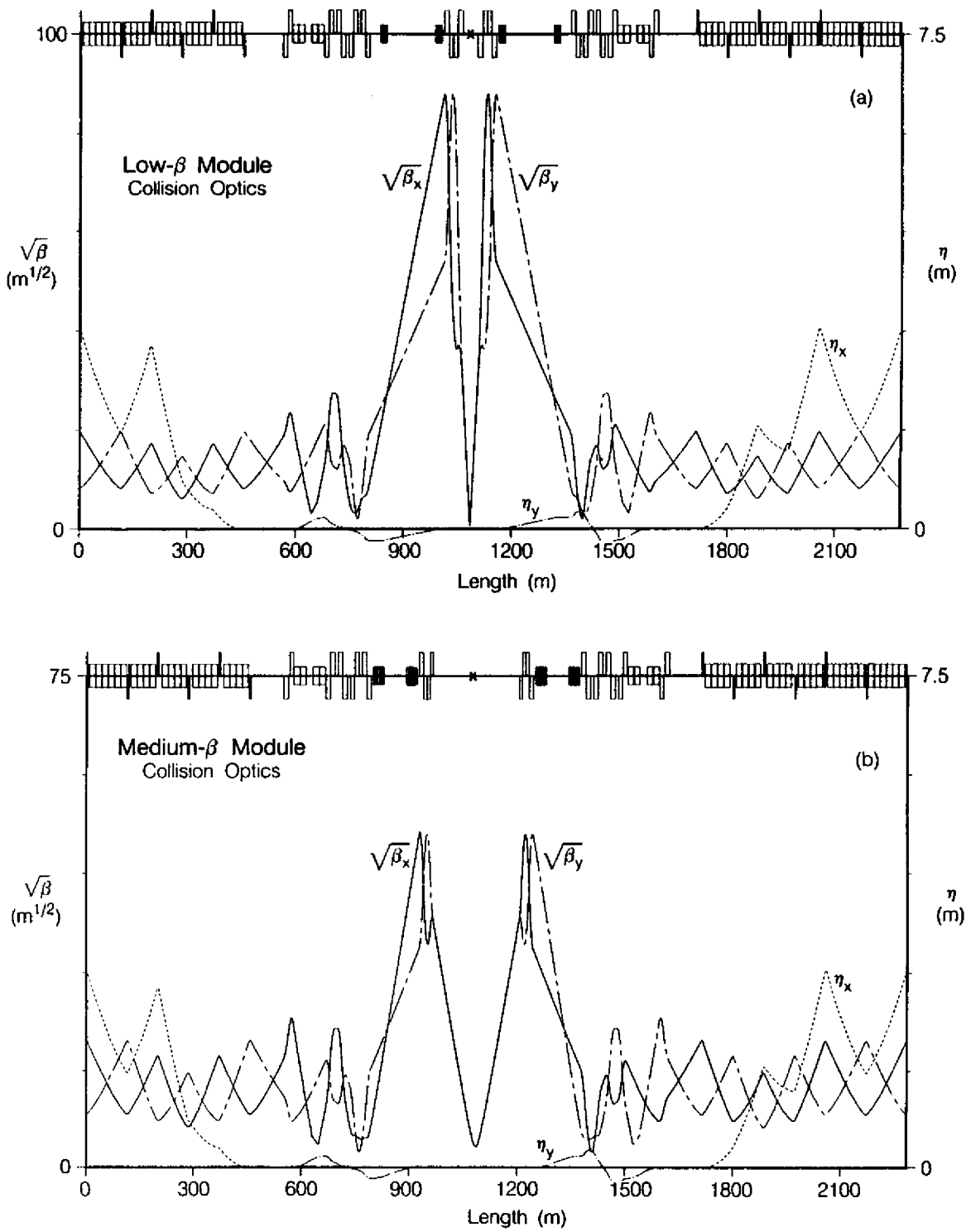

Fig. 7. (a) Low-β module; collision optics. (b) Medium-β module; collision optics.

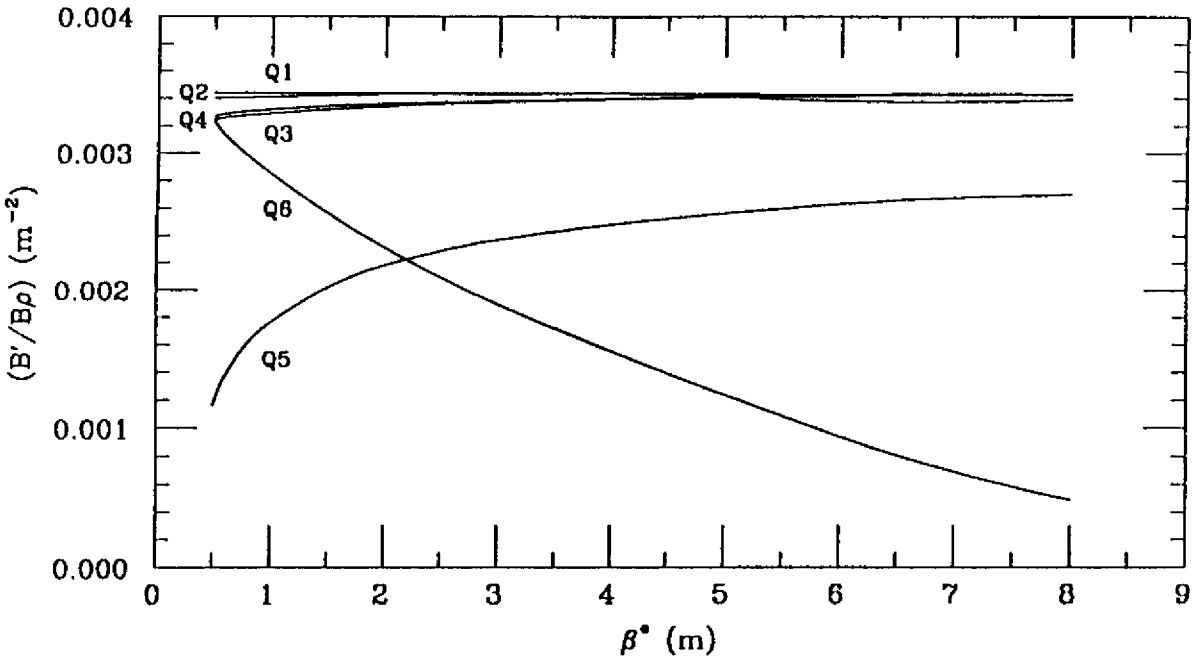

Fig. 8. Low-β module; quadrupole tuning curves.

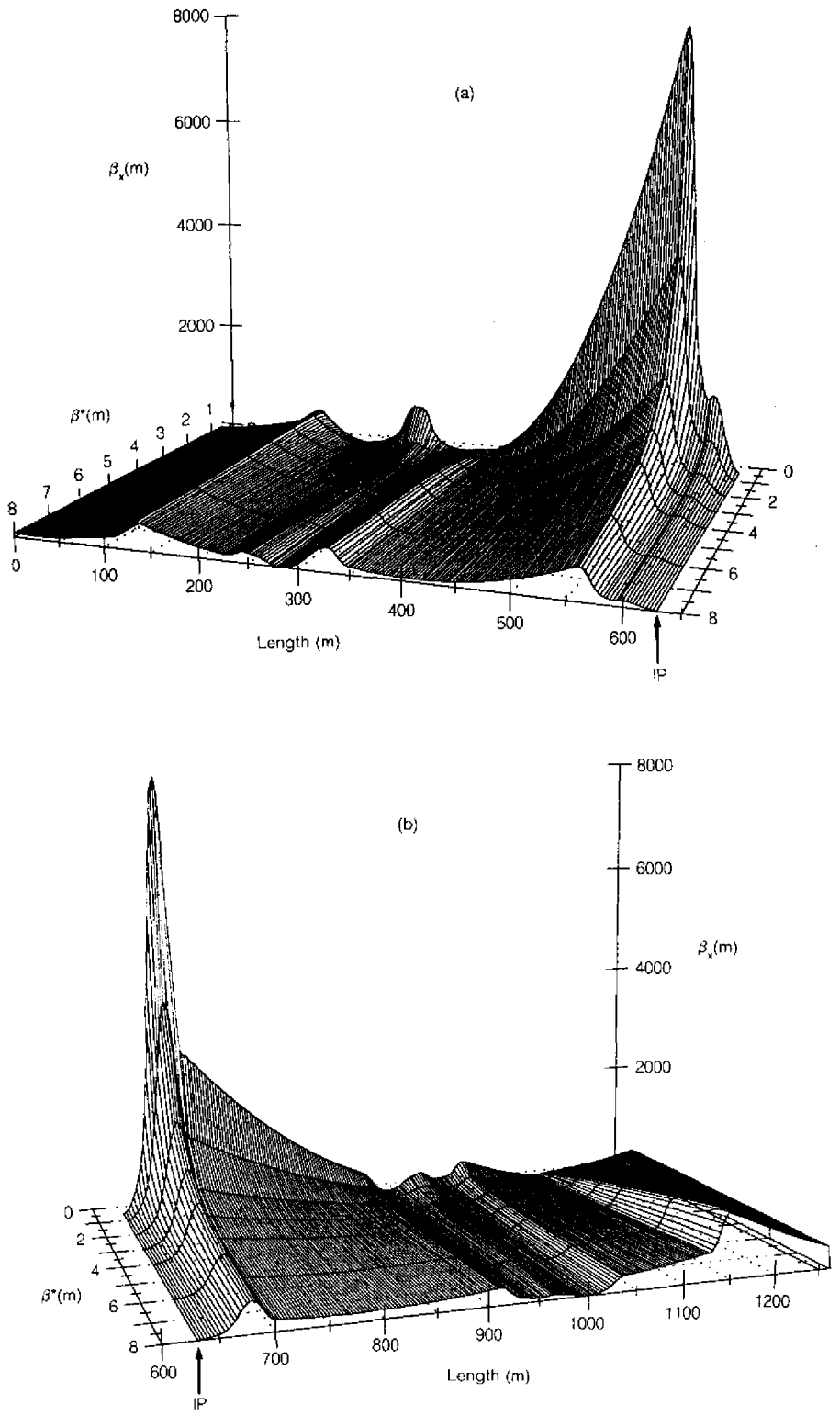

Fig. 9. Low-β module; horizontal beta function during tuning. (a) Left-hand side of module. (b) Right-hand side of module.

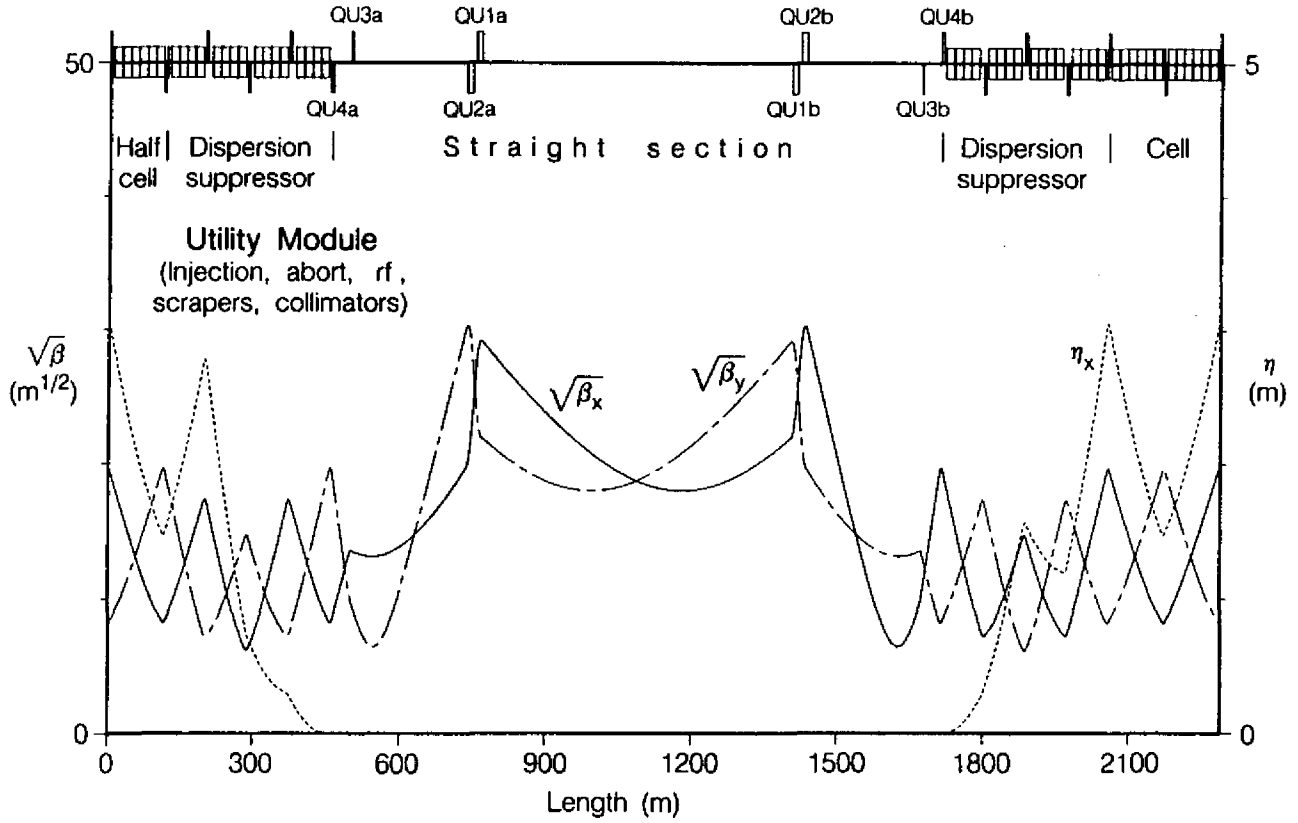

Fig. 10. Utility module.

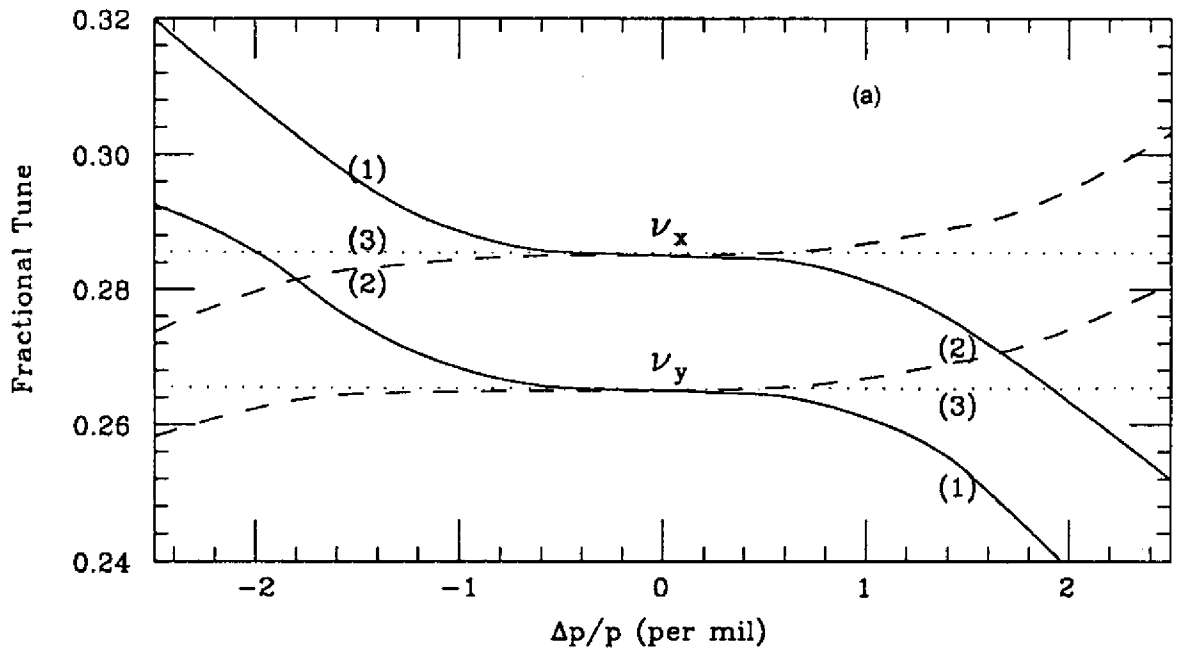

Fig. 11. (a) Momentum dependence of the SSC for (1) collision, (2) intermediate, and (3) injection optics.

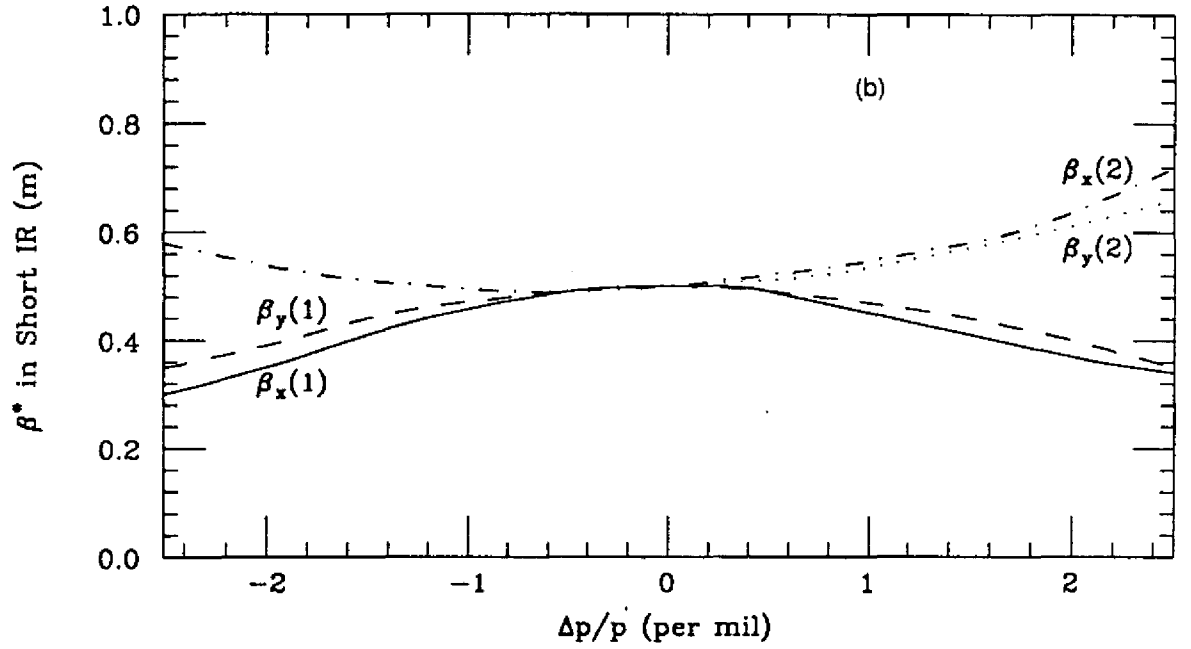

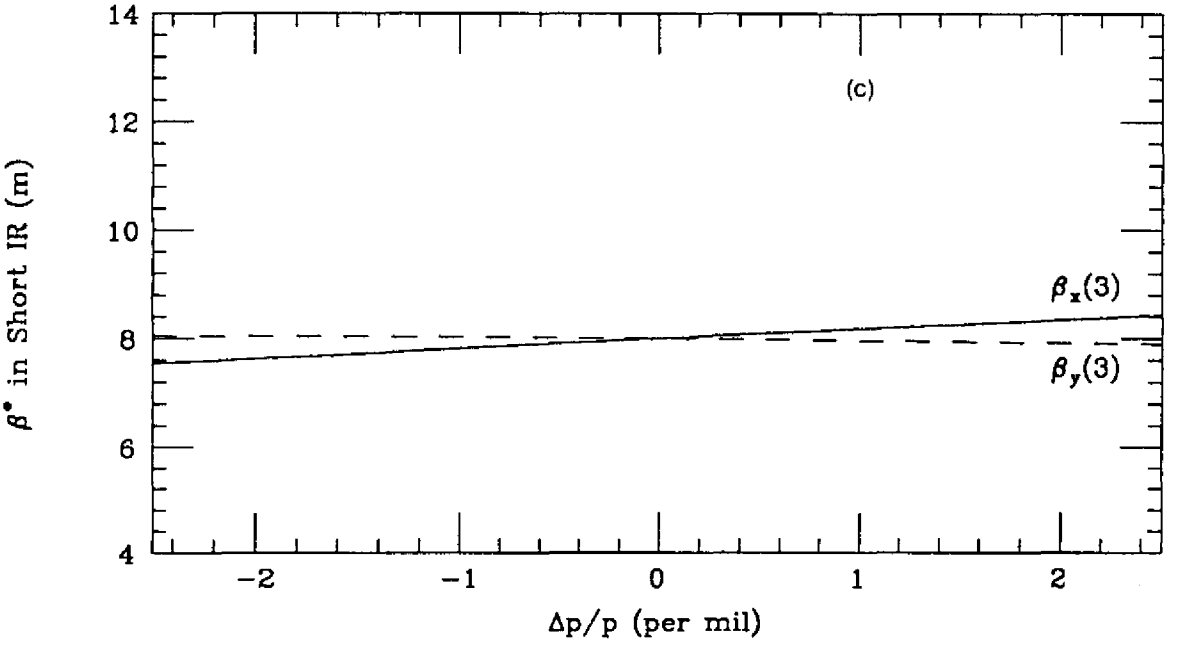

Fig. 11. (b) Momentum dependence of β* in the low-β module for the first two cases. (c) Momentum dependence of β* in the low-β module for the injection optics.

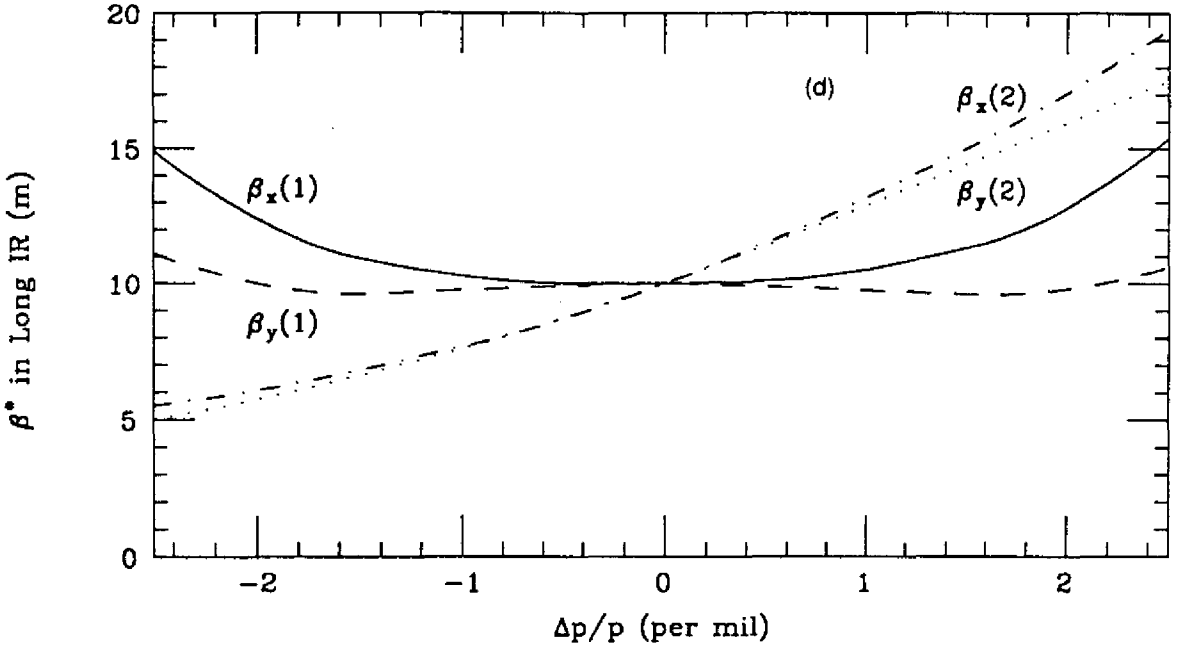

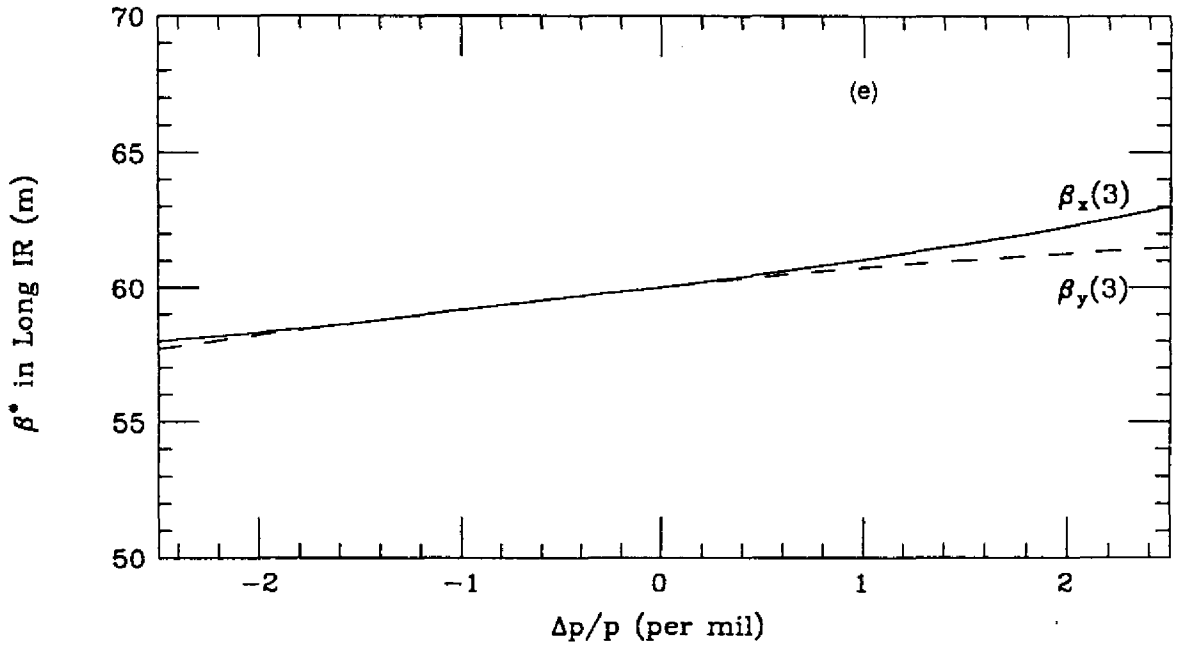

Fig. 11. (d) Momentum dependence of β* in the medium-β* module for the first two cases. (e) Momentum dependence of β* in the medium-β module for the injection optics.

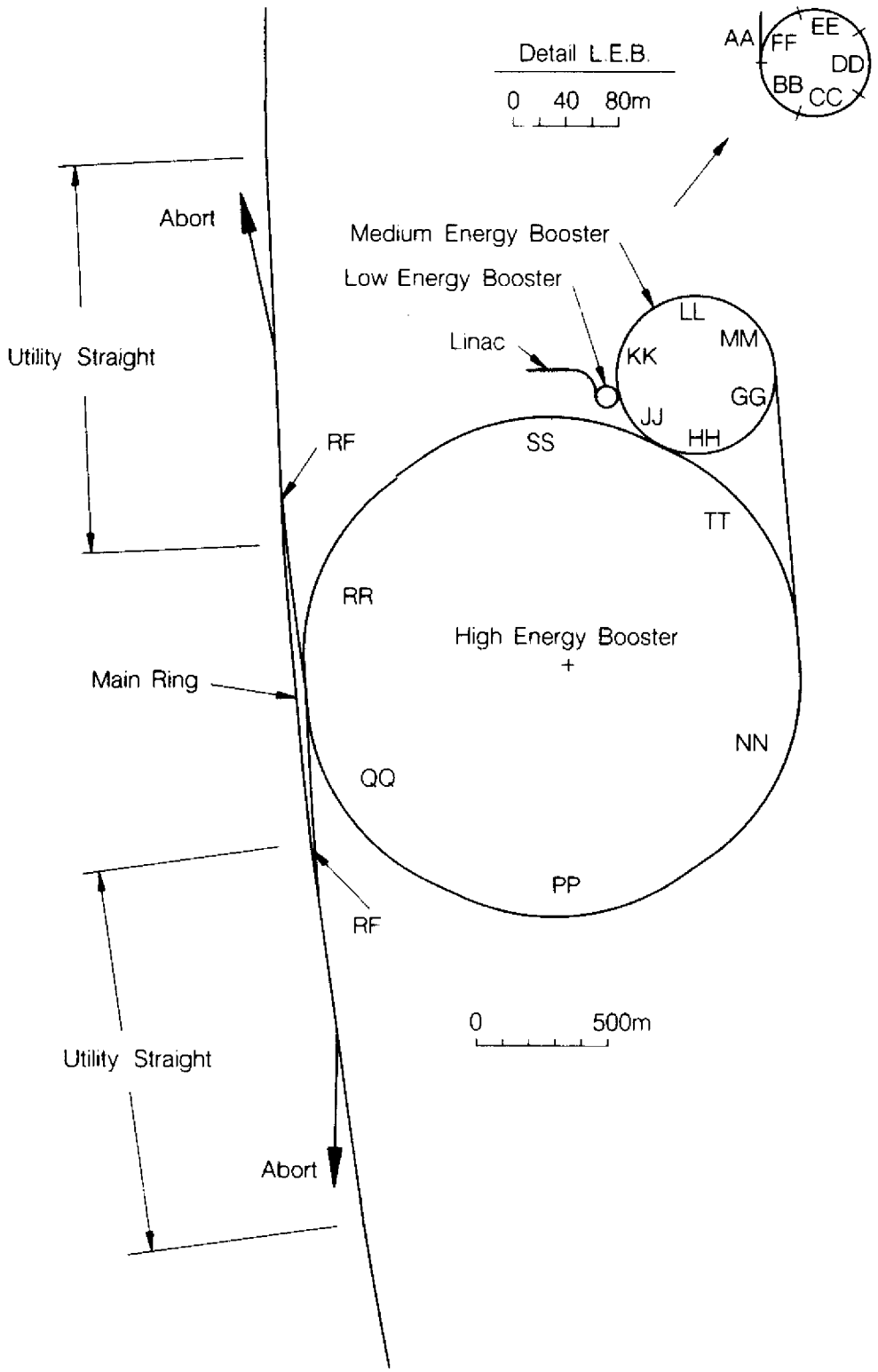

Fig. 12. Layout of the SSC injector complex.

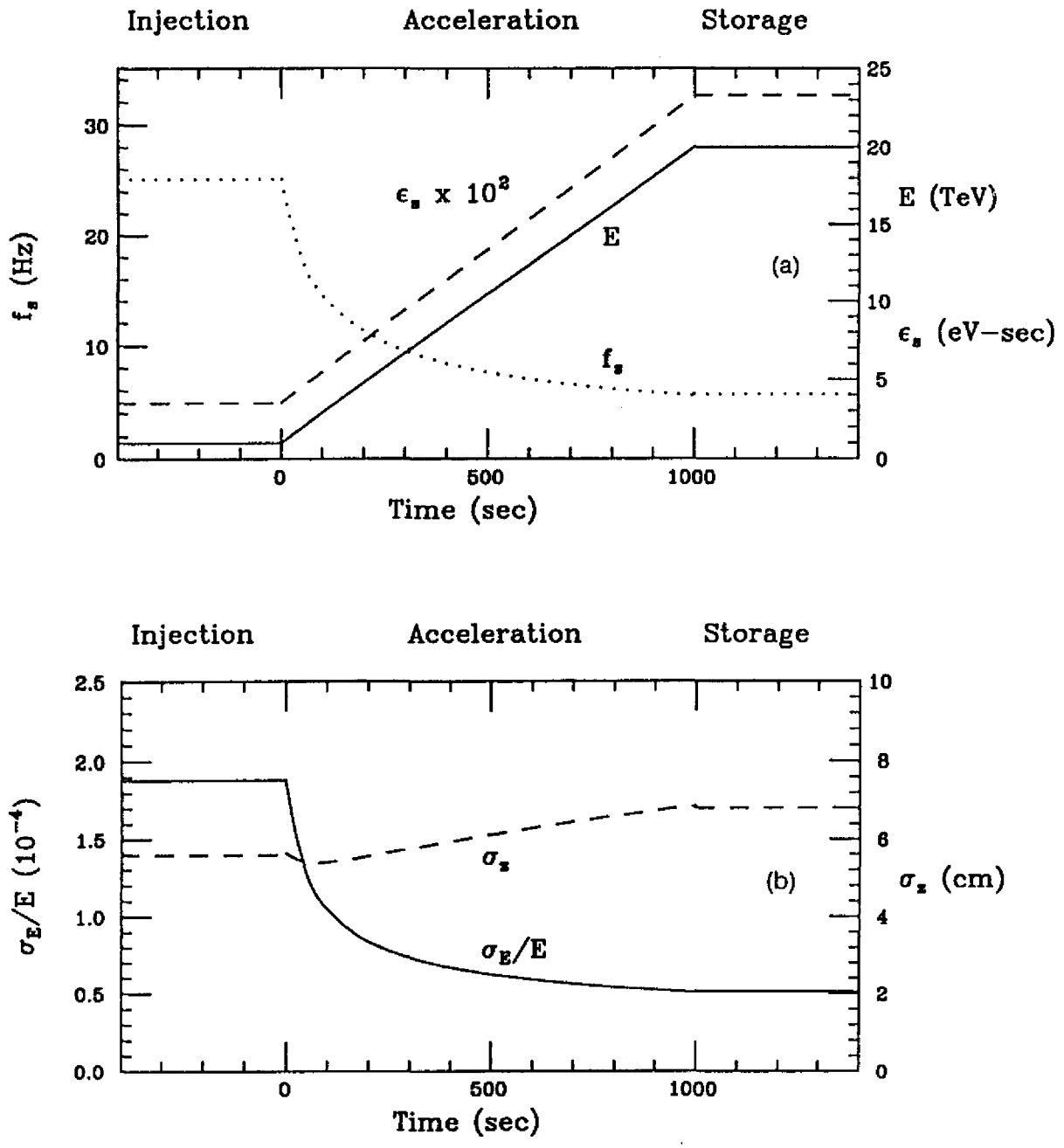

Fig. 13. Variation of rf and beam parameters during the 1000-second acceleration ramp. The peak 354 MHz rf voltage is kept constant at 20 MV. (a) beam energy E, longitudinal emittance $\varepsilon_s = \sigma_E \sigma_t$, synchrotron frequency f_s. (b) rms longitudinal spread σ_z and rms fractional energy spread σ_E/E.

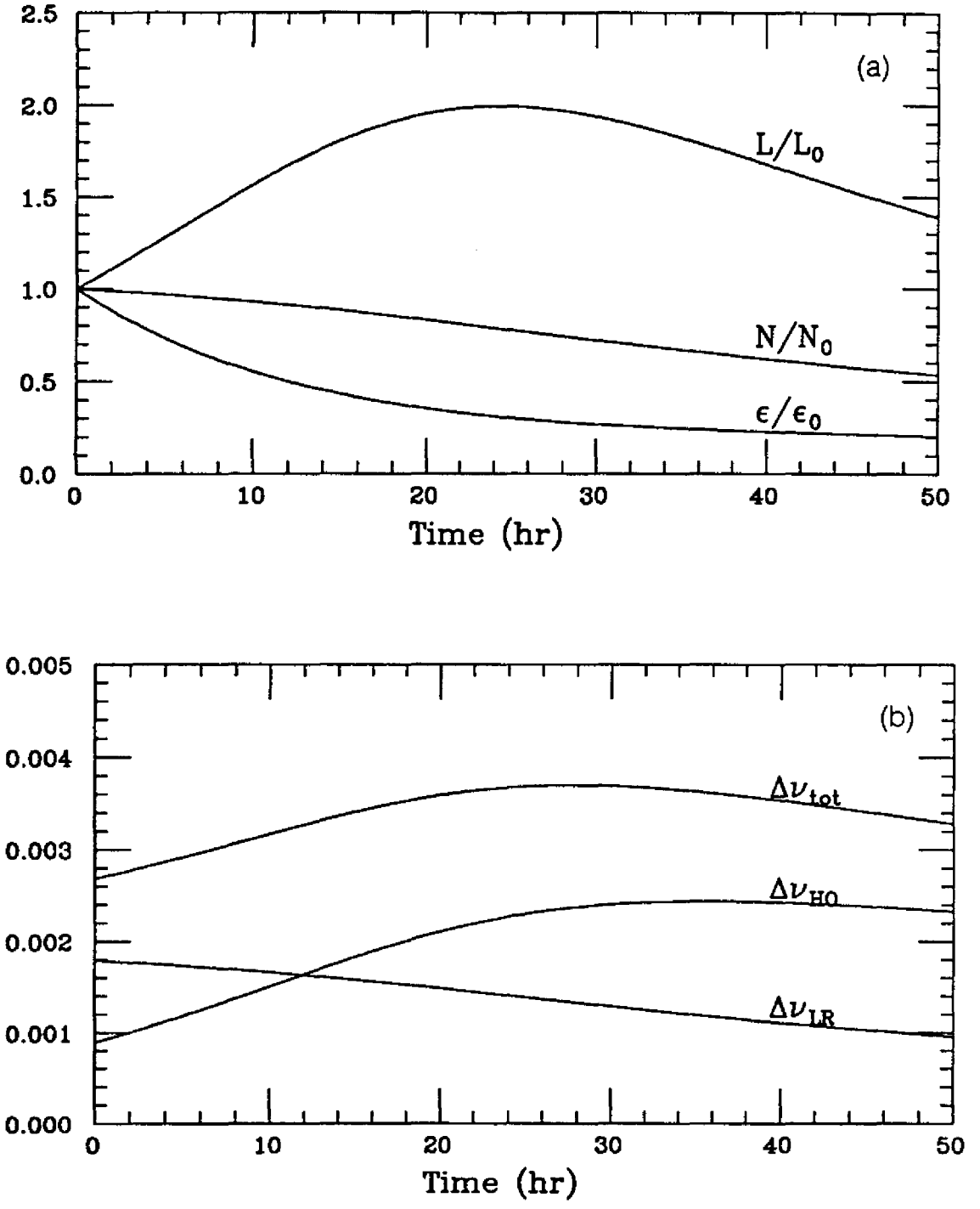

Fig. 14. Time dependence of various quantities during collision. (a) N_B, $\mathcal{L}_1$ and ε, normalized by their initial values. (b) $\Delta\nu_{HO}$, $\Delta\nu_{LR}$ and their sum $\Delta\nu_t$ for the high luminosity interaction points.

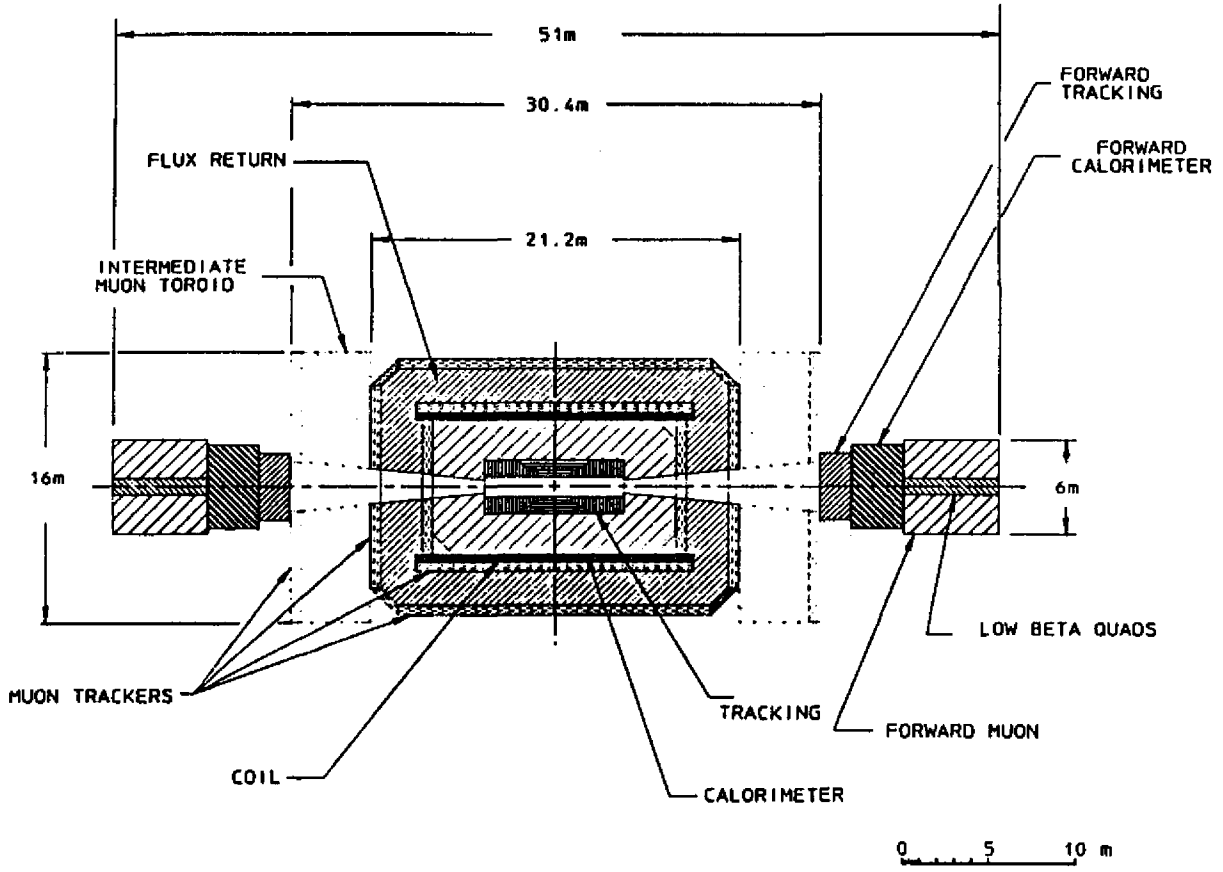

Fig. 15. Large solenoid detector.

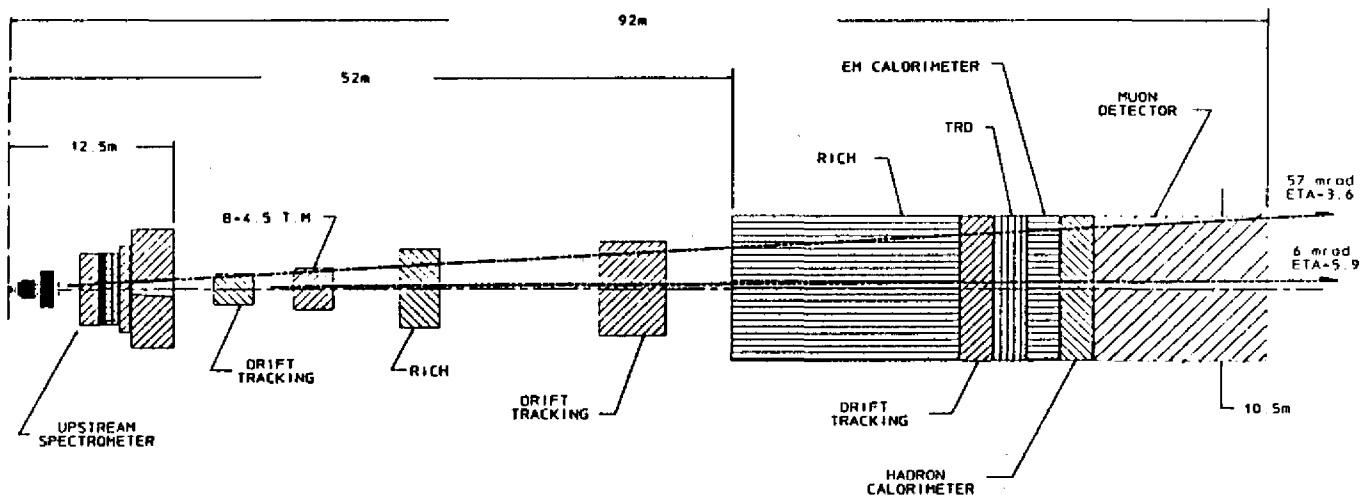

Fig. 16. Downstream beauty spectrometer.